Exploring the Potential of Sub-daily Microwave Remote Sensing Observations for Estimating Evaporation in Forests

Emma Tronquo, Hans Lievens, Susan C. Steele-Dunne, Niko E. C. Verhoest, and Diego G. Miralles

***Abstract*—Terrestrial evaporation (E) plays a crucial role in the water, energy, and carbon cycles and modulates climate change through multiple feedback mechanisms. While process-based models estimate E using satellite-derived drivers, they typically operate at daily or lower temporal resolutions. Key components of E, such as transpiration and interception loss, exhibit strong diurnal variability, especially under water stress and during or shortly after precipitation events. Therefore, capturing the sub-daily variability of these variables is essential for improved process understanding and E monitoring at fine temporal resolutions. Sub-Daily microwave observations offer the potential to resolve these short-term processes while providing all-sky retrievals. The Sub-daily Land Atmosphere INTEractions (SLAINTE) mission, proposed as part of European Space Agency's New Earth Observation Mission Ideas, aims to provide sub-daily Synthetic Aperture Radar (SAR) observations of surface soil moisture (SSM), vegetation optical depth (VOD), and wet/dry canopy state (WDCS). These observations are expected to enhance the estimation of E beyond current capabilities. This study explores the added value of such observations through observing system simulation experiments conducted at four European eddy-covariance forest sites, constraining a sub-daily version of the Global Land Evaporation Amsterdam Model (GLEAM) with synthetic sub-daily microwave observations. Three experiments assess the impact of: 1) sub-daily SSM on bare soil evaporation and transpiration; 2) sub-daily VOD on transpiration; and 3) sub-daily WDCS on interception loss. Results demonstrate that prospective sub-daily microwave data can substantially improve E estimates and its components, showing average relative improvements in terms of ΔRMSE of up to 25% for interception loss when assimilating sub-daily WDCS, and up to 33% for transpiration when using sub-daily VOD. Our results highlight the need for satellite missions that provide sub-daily microwave data to better understand forest responses to environmental stress.**

***Index Terms*—Microwave remote sensing, synthetic sub-daily observations, terrestrial evaporation.**

I. Introduction

TERRESTRIAL evaporation (E), i.e., the loss of water vapor from land to the atmosphere, is a key variable of the climate system that links the water, energy, and carbon cycles [1]. Despite the fact that around two-thirds of the precipitation over land is evaporated back into the atmosphere [2], E remains the most uncertain global water flux [3], especially in terms of the partitioning into its different components (i.e., bare soil evaporation E_{b}, transpiration E_{t}, interception loss E_{i}, open-water evaporation E_{w}, and sublimation E_{s}) [4], [5]. With rising temperatures and changing vegetation and water availability patterns due to climate change, changes in E trends are expected, albeit with strong regional differences [6], [7], [8]. On average, global E has been increasing in recent decades due to a combination of warming and greening [6], [8], [9], [10], [11], and these trends are expected to continue into the future, fostering the intensification of the global hydrological cycle [8], [12], [13]. Changes in E can have far-reaching impacts on agriculture and water management [14], [15], and they can also influence the occurrence of hydro-climatic extreme events (such as droughts, floods, and heatwaves) through land–atmosphere feedbacks [16]. However, the magnitude of global E, its regional trends, and short-term variability remain uncertain, and thus their implications for water management, forest health, agriculture, and climate [16], [17], [18]. Forest ecosystems require particular attention in this regard. They play a dominant role in regulating surface energy and water fluxes, intensifying or dampening warming depending on the forest type and background climate, and contributing substantially to the global water and carbon cycles [19]. In Europe, forests cover large fractions of the landscape and exert a strong control on regional E patterns, making accurate estimation of E and its different components essential.

Despite its importance, estimating E over large forests is challenging, since it cannot be observed directly by satellite sensors [17], [20]. Different statistical and process-based models have been proposed in recent decades to estimate E by

Received 11 August 2025; revised 11 December 2025; accepted 22 March 2026. Date of publication 2 April 2026; date of current version 29 April 2026. The work of Diego G. Miralles was supported by the European Research Council (ERC) via the HEAT Consolidator under Grant 101088405. The work of Hans Lievens was supported by the STEREO IV research program of BELSPO via the WAVETRAX project under Grant SR/00/416. The work of Susan C. Steele-Dunne was supported via a Talent Programme (Vici) under Grant 20714 financed by the Dutch Research Council (NWO). This work was supported by the European Space Agency (ESA), New Earth Observation Mission Ideas (NEOMI), project under Grant 4000139242/22/NL/SD. *(Corresponding author: Emma Tronquo.)*

Emma Tronquo is with the Department of Geoscience and Remote Sensing, Delft University of Technology, 2628 CN Delft, The Netherlands, and also with Hydro-Climate Extremes Lab (H-CEL), Ghent University, 9000 Gent, Belgium (e-mail: E.Tronquo@tudelft.nl).

Hans Lievens, Niko E. C. Verhoest, and Diego G. Miralles are with Hydro-Climate Extremes Lab (H-CEL), Ghent University, 9000 Gent, Belgium (e-mail: Hans.Lievens@UGent.be; Niko.Verhoest@UGent.be; Diego.Miralles@UGent.be).

Susan C. Steele-Dunne is with the Department of Geoscience and Remote Sensing, Delft University of Technology, 2628 CN Delft, The Netherlands (e-mail: S.C.Steele-Dunne@tudelft.nl).

Digital Object Identifier 10.1109/JSTARS.2026.3679245

combining remotely observable variables related to this flux of water [21], [22]. Furthermore, satellite-based E retrieval estimates remain highly uncertain. Most approaches rely on optical and thermal data, from e.g., ECOSTRESS [23] or Sentinel 2/3 [24], resulting in noncontinuous E records due to cloud cover. In addition, thermal data are mostly sensitive to temperature, rather than actual soil moisture, even though the latter is a key driving factor for E [25]. While recent studies have demonstrated the potential of high spatial resolution optical sensors to retrieve canopy water content (e.g., [26]), these approaches remain constrained by their limited temporal revisit, often several days, and by their strong dependence on cloud-free conditions, which reduces the continuity and reliability of the retrieved products. Moreover, E_{i} cannot be derived from thermal and optical data, since it occurs mostly at times of cloud cover. Therefore, while future missions like Land Surface Temperature Monitoring (LSTM) [27] and Thermal infraRed Imaging Satellite for High-resolution Natural resource Assessment (TRISHNA) [28], or existing CubeSat constellations [29], hold great potential to estimate E at high spatial resolutions, they still present challenges in terms of temporal resolution, coverage, continuity, sensitivity to drivers like soil moisture, or capacity to derive E_{i}.

In contrast to thermal and optical retrievals, microwave retrievals are not dependent on cloud-free conditions and can be used to generate continuous records. Moreover, microwave observations are directly sensitive to changes in soil moisture, internal vegetation water content, and the water content present on vegetated surfaces due to dew and precipitation (or irrigation) [30], [31], [32]. Process-based prognostic models making use of microwave data have been developed in recent years. For instance, Purdy et al. [33] assimilated Soil Moisture Active Passive (SMAP) data to improve E estimates based on the Priestley–Taylor Jet Propulsion Laboratory (PT-JPL) model. The Penman–Monteith–Leuning (PML) model used precipitation data, partly based on passive microwave observations, to estimate E_{i} [6]. Likewise, the High resOlution Land Atmosphere Parameters from Space (HOLAPS) framework used passive microwave-based precipitation to compute a soil water balance and E_{i} [34]. However, the reliance on microwave data is the largest in the case of the Global Land Evaporation Amsterdam Model (GLEAM) [35], which leverages microwave observations of surface soil moisture (SSM), vegetation optical depth (VOD), and precipitation, which are used as forcings to estimate E. The main limitation of the most common sources of microwave observations, i.e., radiometry and scatterometry, is their relatively low spatial resolution (several kilometers), insufficient to meet E data requirements for local-scale water management, agriculture, ecosystem monitoring, and weather prediction [17]. As an alternative, Synthetic Aperture Radar (SAR) microwave data can be used to overcome the spatial resolution issues of radiometers and scatterometers. In fact, Rains et al. [36] recently illustrated the potential of assimilating backscatter observations from Sentinel-1 into GLEAM to improve modeled soil moisture, while Martens et al. [37] tested the applicability of GLEAM at fine spatial resolutions.

In addition to high spatial resolutions, high temporal resolutions are also relevant for E monitoring over forests. Several studies (e.g., [38], [39], [40]) have shown that E exhibits a pronounced diurnal hysteresis, with higher E rates during the morning compared to the afternoon, especially in dry conditions. This hysteresis arises from the nonlinear dynamics of water transport within the soil–plant–atmosphere continuum throughout the day. E_{t} occurs primarily during the diurnal opening of stomata to carry out photosynthesis, decreasing the leaf water potential, which makes water move from the soil through the plant water column to the leaves. This moisture redistribution is a highly nonlinear process and shows a strong daily cycle, with increasing atmospheric water demand during the day, leading to enhanced E_{t}, and recharge of water from the soil during the night. To realistically represent this natural variability of E_{t}, there is a need to monitor how vegetation responds to diverse sources of stress at sub-daily scales [17]. Moreover, fine temporal resolutions are also needed for E_{i}, which shows a high intraday variability, mainly concentrated during precipitation events and shortly after. Sub-daily microwave observations are highly sensitive to canopy surface wetness, as demonstrated by Vermunt et al. [31], enabling the detection of E_{i} at fine temporal scales. Having observations distributed throughout the day would allow for more accurate modeling of E_{i} by better constraining canopy drying time, storage capacity, and the filling and draining dynamics [7], [41].

Despite natural E processes occurring at sub-daily time scales, E remote sensing has typically focused on daily to annual scales, restricted by the availability of satellite observations. This limitation extends to current and prospective SAR missions, such as Sentinel-1, the Argentinean Satélite Argentino de Observación COn Microondas (SAOCOM), NASA-ISRO SAR (NISAR), and Radar Observing System for Europe in L-band (ROSE-L), which provide only one snapshot every few days. Although most satellites are in sun-synchronous orbit, and their ascending and descending overpasses sample at different particular times of day, these acquisitions do not occur within the same day at a given location, resulting in irregular and infrequent sampling that is insufficient to accurately represent sub-daily dynamics. In this regard, sub-daily radar observations would provide a means to inform about the redistribution of moisture within the soil–plant–atmosphere continuum during the day, and as such enable an accurate estimation of E_{t} and E_{i}, while providing all-skies E retrievals [31], [42], [43], [44], [45], [46].

The research presented here has been performed to support the development of the Sub-daily Land Atmosphere INTEractions (SLAINTE) mission idea. SLAINTE is a European Space Agency (ESA) New Earth Observation Mission Idea (NEOMI) concept aiming to fill a critical observation gap by focusing on the fast dynamics of water status in the soil–plant–atmosphere continuum [47]. SLAINTE foresees a constellation of at least three Low Earth Orbit monostatic L-band SARs, providing observations separated by 6 hours and a repeat cycle of 3 days [48]. One of the objectives of SLAINTE is to improve the process understanding of E and its different components, and to reduce uncertainties in their estimates. Specifically, 1) sub-daily retrievals of SSM can be used to improve the estimation of E_{b} and E_{t}, 2) sub-daily retrievals of VOD can be used to improve E_{t} estimates, and 3) sub-daily binary retrievals of canopy wetness state, i.e., wet/dry canopy state (WDCS), can inform about the

canopy drying time and canopy storage capacity, and therefore improve E_i estimates. The availability of sub-daily data would pave the way toward more proactive management in hydrology, forestry, agriculture, and climate science.

To study the potential of sub-daily SLAINTE-like observations for improving E estimates, synthetic microwave observations are employed in so-called observing system simulation experiments (OSSEs) [49], [50]. OSSEs are typically used to test the potential impact of prospective observations by assimilating synthetic, rather than real, observations into a model. These synthetic observations are simulated from a realistic nature run (NR), representing the "true" state [50]. A simulation study by Holtzman et al. [51] used an OSSE set-up to quantify the potential utility of different observation temporal frequencies of passive microwave sensors in constraining plant hydraulics in a land surface model to improve plant water potential, soil moisture, E, and gross primary productivity estimates. The results highlighted the added value of observing four times a day, compared to twice a day, to better capture diurnal fluctuations in plant water potential and corresponding fluxes. In this manuscript, we implement a total of three experiments using a sub-daily implementation of GLEAM to assimilate synthetic observations of sub-daily SSM, sub-daily VOD, and sub-daily information about the presence of water on the vegetation canopy (i.e., WDCS). Forecast results of the experimental assimilation runs are compared to a control run (CR), which represents the current state-of-the-art in global E modeling. Because this run reflects what is presently available for operational E modeling, CR provides a realistic baseline against which the added value of assimilating sub-daily SAR observations can be assessed.

The aim of this study is to determine the degree to which sub-daily SAR observations (such as those proposed by SLAINTE) have the potential to improve the accuracy of E and its different components in forested ecosystems. An OSSE is designed to investigate the potential impact of sub-daily SAR observations on E estimates at four forest study sites in Europe, by means of a twin experiment, in which the simulation results after assimilating the synthetic sub-daily microwave observations are compared with the simulated synthetic truth across various temporal observation frequencies. Thus, the focus of this study is to assess the relative improvement obtained when assimilating these synthetic sub-daily observations compared to a baseline representing the current state-of-the-art in E modeling, rather than fine-tuning or optimizing the performance of the sub-daily E model itself.

The remainder of this article is organized as follows. Section II describes the E model (GLEAM) used in the experimental setup, including both the default (daily) setting and modified (sub-daily) settings. In Section III, an overview is given about the experimental set-up, including a description of the study sites, forcing data to the E model, and a detailed outline of the OSSE-based system set-up. Results of the experiments are listed in Section IV for first the validation of NR and CR and then the impact of assimilating sub-daily SSM, sub-daily VOD, and a sub-daily WDCS, and their combined impact on E modeling. The findings of this study are discussed in Section V. Finally, Section VI concludes this article.

II. Model

GLEAM, originally developed by Miralles et al. [35], is used to estimate E and its main components (E_t, E_b, E_i, E_s, and E_w). GLEAM is a state-of-the-art remote sensing-based E model that offers advantages over other E models, including the use of microwave remote sensing observations of soil moisture and VOD, which enables the computation of E to all skies. For this study, a recent version of the model, i.e., GLEAM-Hydro [52], is adapted to work at sub-daily (3-hourly) resolution, and the model experiments are executed at four forest study sites (see Section III-A).

A. Default Settings – GLEAM-Hydro

GLEAM-Hydro builds upon GLEAM version 3 [55], adapting it to account for plant access to groundwater, and thus providing a more realistic process representation of E under water-limited conditions [52]. GLEAM-Hydro, like previous versions of GLEAM, computes E estimates at daily time steps. First, potential evaporation is computed by employing a Priestley and Taylor equation [56], utilizing temperature and radiation data. Actual E_t and actual E_b are derived by constraining potential evaporation estimates with an empirical stress factor (S), which is a function of soil and vegetation water content, the latter accounted for by VOD. E_i is computed independently based on Gash's analytical model [35]. For E_s and E_w, the model assumes potential rates parameterized specifically for these land covers. The sum of these components (i.e., E_t, E_b, E_i, E_s, and E_w) yields E.

The soil water balance module that is implemented in GLEAM-Hydro consists of a three-layer bucket and relies on observed precipitation. A fourth layer, i.e., a linear reservoir model, is used to represent groundwater. An E_t partitioning approach was introduced to estimate groundwater-sourced evaporation to realistically represent E under water-limited conditions. The soil module assimilates SSM, brightness temperature, and/or backscatter observations to enhance the representation of root-zone soil moisture (RZSM) [36], [55], [57]. In the case of bare soils, SSM is the only variable that determines S used to limit E below its potential. For vegetated areas, RZSM is empirically combined with VOD to determine the transpiration stress. A full description GLEAM-Hydro can be found in Hulsman et al. [52] and Martens et al. [55].

B. Sub-Daily Modified Settings

To assess the potential of sub-daily microwave observations for estimating E, GLEAM-Hydro is modified to work at sub-daily (3-hourly) resolution (hereafter referred to as sub-daily GLEAM). A schematic representation of the sub-daily E model is provided in Fig. 1(a). This adaptation involves adjusting the data assimilation routine to allow for the use of sub-daily forcing data, and the inclusion of synthetic observations of sub-daily SSM, WDCS, and VOD (see Section III-B for more details). Static model parameters are adapted to the sub-daily scale when required. In addition, the original E_i scheme is replaced by a model that allows the estimation of E_i at sub-daily time steps for both tall and short vegetation. This sub-daily E_i model

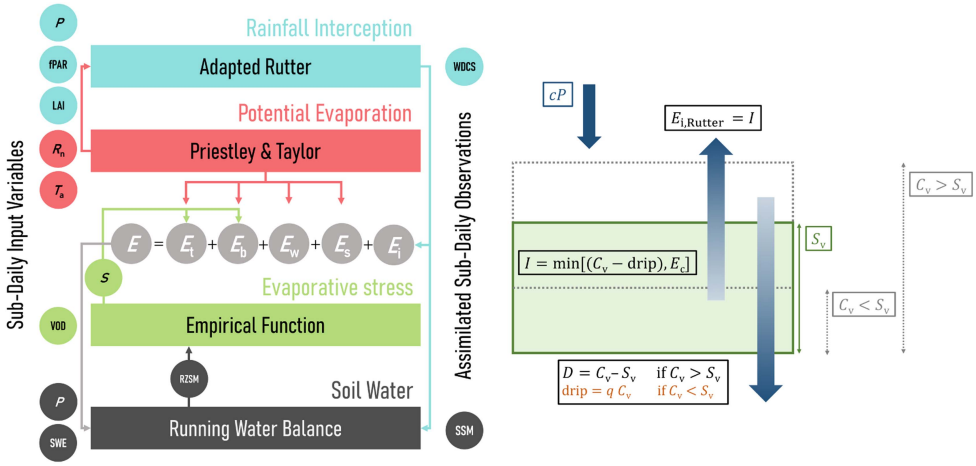

(a) (b)

Fig. 1. Schematics of the sub-daily version of GLEAM. (a) General model structure to estimate E, E_t, E_b, E_w, E_s, and E_i. Sub-daily inputs include precipitation (P), photosynthetically active radiation (fPAR), leaf area index (LAI), near-surface net radiation (R_n), air temperature (T_a), VOD, and snow water equivalent (SWE). Sub-daily SSM and binary WDCS observations can be assimilated. RZSM is calculated in the soil water module and used to determine the evaporative stress (S). (b) The adapted Rutter's conceptual interception model [53], [54], with c the vegetation cover, P the precipitation, C_v the vegetation water storage, S_v the vegetation storage capacity, D the drainage of water, q the drip factor, E_c the wet canopy evaporation rate, and I the interception loss.

is an extension of the recent E_i model presented by Zhong et al. [58], adapted following a Rutter approach [53], [54] to make it applicable at sub-daily scales. This sub-daily E_i scheme tracks the water storage on the canopy and stems per time step, by calculating a running mass balance considering rainfall, throughfall, evaporation, and changes in the canopy storage, whereby the final output is the evaporation from wet vegetated surfaces, i.e., E_i.

Fig. 1(b) provides a graphical overview of the sub-daily E_i model with c the vegetation cover fraction, cP representing the precipitation falling on the vegetation, C_v the vegetation water storage, S_v the vegetation storage capacity, D the drainage of water, and E_c the wet canopy evaporation rate. In addition to the original Rutter model [53], [54], a drip component is included to account for water dripping from the canopy before saturation is reached (drip $= q * C_v$, with drip factor $q = 0.3$). This value was found to produce realistic daily interception amounts that compare well with alternative interception models, such as Zhong et al. [58]. The vegetation water storage (C_v) can be further constrained through the assimilation of potential sub-daily WDCS observations, providing additional information on canopy wetness dynamics. The interception model is driven by satellite-observed vegetation dynamics, potential evaporation, and precipitation. To parameterize this Rutter-based model, we use leaf and stem storage capacity estimates reported by Zhong et al. [58], who derived these parameters from an extensive global compilation of field campaigns covering a wide range of plant functional types. By linking these field-based values to the MODerate-resolution Imaging Spectroradiometer (MODIS) land cover product following the International Geosphere-Biosphere Programme (IGBP) classification, Zhong et al. [58] generated a global gridded dataset of canopy storage capacities. For each forest study site, we extract the corresponding grid cell and use its associated vegetation parameters to estimate E_i.

III. Experimental Set-Up

A. Study Sites

To assess the impact of sub-daily microwave observations in estimating E, assimilation experiments are conducted at four eddy-covariance forest sites. The selection of these sites aims to span various climatic regimes and forest types within Europe. The geographical location of the forest sites, along with some graphics of the measurement tower and forest types, is depicted in Fig. 2. This selection comprises the following.

1) *Hainich (DE-Hai):* The site is located in the Hainich National Park in Thuringia, Germany, and is surrounded by an old-growth mixed deciduous broadleaf forest. The forest exhibits characteristics of an unmanaged, uneven-aged (with a maximum tree age of around 265 years), and structurally diverse forest [59]. The climate at the study site is classified as humid continental with warm summers. Mean annual temperature is 8.34 °C, and mean annual precipitation is 744 mm (source: ICOS [60], FLUXNET [61]). The data record length spans from January 2010 to December 2020.
2) *Majadas del Tiétar North (ES-LM1):* The site is located in a holm oak grove ecosystem in Las Majadas de Tiétar, Caceres (Spain). The tree canopy coverage at the sites is ∼20% and traditional woodland grazing takes place regularly. The climate is continental Mediterranean with mild winters, with mean annual temperature of 17.2 °C, and mean annual precipitation of 670 mm (source: ICOS [60]). The data record spans from January 2014 to December 2020.
3) *Puéchabon (FR-Pue):* The site is located in l'Hérault, southern France. The main ecosystem is evergreen broadleaf forest, dominated by dense woody vegetation with percent cover >60% and mean tree height of

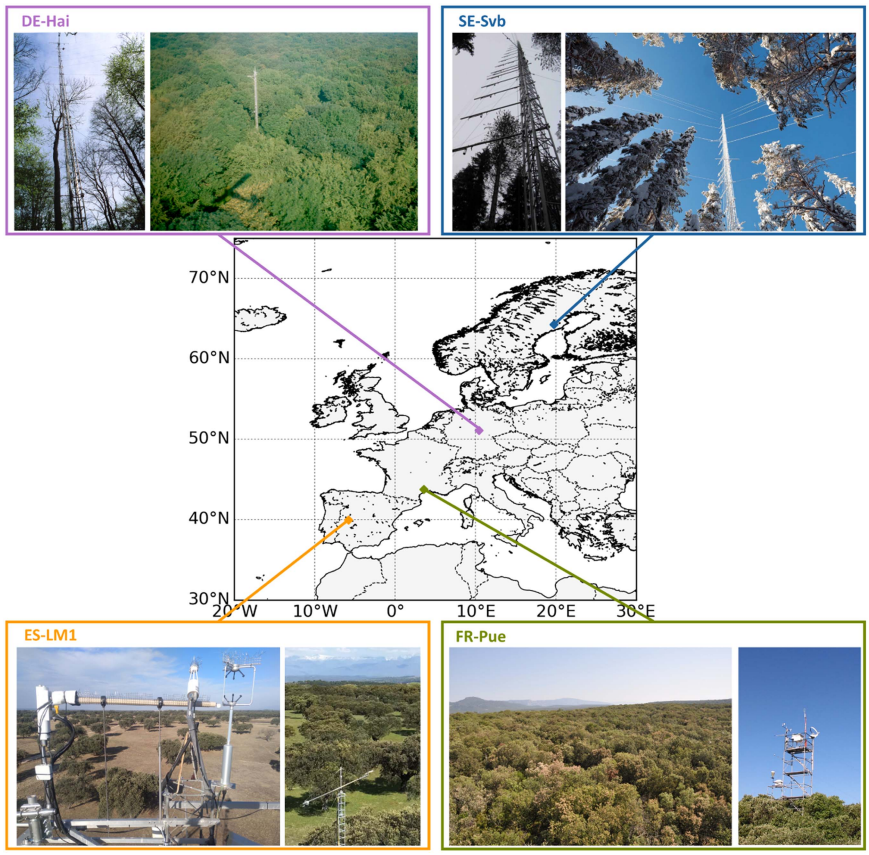

Fig. 2. Geographical location of the four eddy-covariance forest sites spread across Europe. Source: ICOS [60] and FLUXNET [61].

5.5 m [62]. The Puéchabon forest has a Mediterranean-type climate, with mean annual temperature of 13.5 °C and mean annual precipitation of 883 mm (source: ICOS [60], FLUXNET [61]). The data record length of this site spans from January 2010 to December 2014.

4) *Svartberget (SE-Svb):* The site is located northwest of the city Umeå (Sweden). The ecosystem is an evergreen needleleaf forest, and the landscape of the site is characterized by ridges, valleys, and lakes stretching from northwest to southeast. The station is located within the Svartberget experimental forest. It is characterized by a subarctic climate regime, with mean annual temperature of 1.8 °C and mean annual precipitation of 614 mm (source: ICOS [60]). The data record length of this site spans from January 2014 to December 2020.

B. Data

Table I lists all data products used in the computation of sub-daily GLEAM to perform the experiments. Data products are rescaled to a resolution of 0.1° or 0.25° by means of bilinear interpolation, depending on the experiment type (see Table II).

1) Meteorological Forcing: In situ measurements of precipitation, air temperature, and near-surface radiation fluxes measured at eddy-covariance towers of the FLUXNET2015 [61] and the ICOS [60] network are used as meteorological forcing variables in NR, to represent "true" E at the study-sites (see Section III-C). The meteorological variables are measured at the four forest eddy-covariance sites listed in Section III-A. For the OSSEs, ERA5 meteorological data [63] are used as forcing, assuming a higher uncertainty compared to in situ measurements. In addition, latent heat flux measured at the

TABLE I
OVERVIEW OF FORCING VARIABLES AND CORRESPONDING DATASETS USED IN THE COMPUTATION OF SUB-DAILY GLEAM, WITH THEIR ORIGINAL TEMPORAL AND SPATIAL RESOLUTION

Forcing variables	Dataset	Resolution
Nature run		
Precipitation	FLUXNET2015 & ICOS	3h; site
Air temperature	FLUXNET2015 & ICOS	3h; site
Radiation	FLUXNET2015 & ICOS	3h; site
Experiments		
Precipitation	ERA5	1h; 0.25°
Air temperature	ERA5	1h; 0.25°
Radiation	ERA5	1h; 0.25°
fPAR	MODIS MCD15A3H v6	4d; 500m
LAI	MODIS MCD15A3H v6	4d; 500m
VOD	VODCA	Daily; 0.25°
Vegetation fractions	MEaSUREs VCF5KYR_001	Yearly; 0.05°
	MOD44B v6.1	Yearly; 250m
SWE	GLOBSNOW v3	Daily; 0.25°
Soil properties	HiHydroSoil v2	250m
	IGBP-DIS	0.25°

TABLE II
E EXPERIMENTS

Code	Experiment description	SSM DA	WDCS DA	VOD sub-daily	Forcing Data					
					R_n	T_a	P	SWE	VC	SP
NR	Nature run to yield synthetic truth and pseudo-observations (E, E_i, E_t, E_b, SSM and WDCS)	X	X	✓	●	●	●	●	●	●
CR	Control run to benchmark experiments, representing state-of-the-art in global E modeling	X	X	X	●	●	●	●	●	●
SM3–SM24	Assimilation of SSM every 3h, 6h, 9h, 12h, 24h	✓	X	X	●	●	●	●	●	●
V3–V12	VOD observation every 3h, 6h, 9h, 12h	X	X	✓	●	●	●	●	●	●
WD3–WD24	Assimilation of WDCS every 3h, 6h, 9h, 12h, 24h	X	✓	X	●	●	●	●	●	●
ALL3–ALL24	Use of all SAR observations at 3h, 6h, 9h, 12h and 24h frequency	✓	✓	✓	●	●	●	●	●	●

Gray dots indicate the use of *in situ* data measured at forest eddy-covariance sites of net radiation (R_n), air temperature (T_a), and precipitation (P). Black dots indicate the use of ERA5 forcing (0.25°). For vegetation cover (VC) and soil properties (SP), red dots indicate the use of MODIS/MEaSUREs, and HiHydroSoil v2 data at high resolution (0.10° and 250 m, respectively). Blue dots indicate satellite data of SWE (GLOBSNOW) and VC (MODIS/MEaSUREs) at coarse (0.25°) resolution, and SP data from IGBP-DIS also at that resolution.

eddy-covariance sites is used as starting point to validate the model (i.e., sub-daily GLEAM). The original temporal and spatial resolution of these forcing data are listed in Table I. All meteorological forcing variables are rescaled to a common 3-hourly resolution, using interval means for all variables except rainfall, for which 3-hourly totals are computed.

2) Land Properties: For the required variables that are not locally measured at the study sites, satellite products are selected; this includes snow water equivalent (SWE), VOD, soil properties (i.e., porosity, field capacity, wilting point, residual, and critical soil moisture), and land cover fractions. GLOBSNOW data [64] are used as a proxy for daily SWE estimates at the study sites, at 0.25° resolution. VOD is acquired from the global long-term microwave Vegetation Optical Depth Climate Archive (VODCA) [65], providing daily VOD time series at 0.25° resolution. Soil properties are based on the dataset HiHydrosoil version 2 [66] for NR, while for the OSSEs a coarser product is used, i.e., Global Gridded Surfaces of Selected Soil Characteristics dataset developed by the Global Soil Data Task Group of the International Geosphere-Biosphere Programme Data and Information System (IGBP-DIS) [67].

Land cover fractions are derived from MOD44B version 6 Vegetation Continuous Fields (VCF) [68] and the Making Earth System data records for Use in Research Environments (MEaSUREs) [69] on an annual basis. A cumulative density function matching approach is applied, which removes systematic differences between the two datasets, and yields a merged consistent data series spanning the full length of the investigation period (see Zhong et al. [58] for a detailed description of the data processing). Both products provide the percentage of each grid cell covered with tall vegetation, short vegetation, and bare ground. Moreover, for the computation of tall and short vegetation fractions in sub-daily GLEAM, satellite-observed vegetation dynamics are taken into account, as was done by Zhong et al. [58]. In this regard, daily fractions of absorbed photosynthetically active radiation (fPAR) are used to inform about canopy structure and density, which enables the calculation of intra-annual dynamics in vegetation cover fractions [58]. This allows us to formulate E_i for tall and short vegetation separately. In the new E_i model, based on Zhong et al. [58], the vegetation storage capacity is assumed to be linearly related to leaf area index (LAI), offering insight into the influence of seasonal phenological changes on E_i. Both fPAR and LAI data are taken from MODIS product MCD15A3H v6 [70]. The original products are rescaled to 0.1° resolution for both tall and short vegetation, and the original 4-day resolution is temporally smoothed to reproduce a daily time series of vegetation cover fractions. Because GLEAM estimates E independently for tall and short vegetation cover fractions, it is essential to represent vegetation parameters (LAI and fPAR) accurately for these two classes. To achieve this, Zhong et al. [58] derived separate vegetation parameter datasets for tall and short vegetation by identifying the purest tall- and short-vegetation pixels within a 0.1° search radius and extracting their respective LAI and fPAR values. Despite resulting in forcing data at coarser nominal resolution, this approach allows GLEAM to better capture the physical processes associated with each vegetation type. The bare soil vegetation fraction is then calculated as the residual fraction of the pixel.

3) Synthetic Sub-Daily Microwave Observations: Although current sun-synchronous microwave sensors provide acquisitions at two particular times of the day via ascending and descending overpasses, no truly sub-daily observations of SSM, VOD, or WDCS are available to date because they revisit each location only every few days. Therefore, synthetic (yet realistic) observations are used in the experiments for this study. To synthetically generate sub-daily (3-hourly) time series of VOD, in situ latent heat flux time series are first normalized, inverted, and then scaled towards the daily VODCA time series, whereby a standard deviation of 20% was assumed to represent the diurnal cycle [71]. This approach is supported by studies showing strong relationships between VOD derived from satellites on the landscape-scale and hydraulic metrics on the plant-scale, such as the leaf water potential [30], [72], as well as by evidence that VOD exhibits a diurnal cycle consistent with the dynamics of the leaf and stem water potential under constant biomass conditions [71]. Together, these findings justify our assumption of an anticorrelation between VOD and latent heat flux when constructing synthetic sub-daily VOD series. As an illustration, Fig. 3 represents the average diurnal VOD cycle for

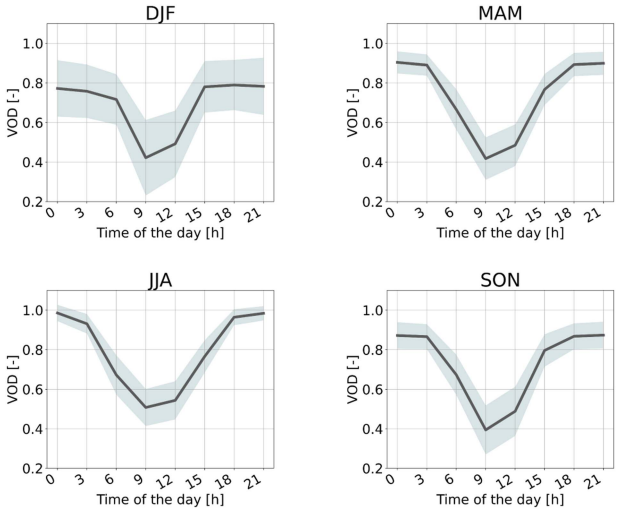

Fig. 3. Diurnal variations of synthetic sub-daily VOD time series (solid line represents the mean, the gray area represents the standard deviation) for the Hainich site in Germany in winter (DJF), spring (MAM), summer (JJA) and fall (SON). The timing of the day is reported in UTC units.

DE-Hai (Germany) over the different seasons. These sub-daily synthetic VOD time series are used in the computation of NR, VOD experiments (V3–V12), and the combined experiments (ALL3–ALL24) (see Table II). For all other experiments, a constant daily VOD value, derived from the VODCA time series is used, at 0.25° resolution.

NR, forced with in situ measured meteorological data, provides a time series of pseudo-observations of SSM at sub-daily resolution (3-hourly). These time series are then perturbed by adding random white noise from a normal distribution with mean 0 and standard deviation of 4 vol%. This noise level represents the threshold measurement uncertainty for SSM retrievals according to GCOS [73]. These synthetic SSM time series are then used in the SSM assimilation experiments (SM3–SM24) and in the combined experiments (ALL3–ALL24) to check the impact of assimilating prospective sub-daily microwave SSM retrievals for the estimation of E, see Section III-C for a detailed description of the assimilation set-up. In addition, a 3-hourly synthetic binary wet/dry canopy mask is defined, based on the time series of simulated E_i from NR. These synthetic WDCS time series reflect whether the canopy is wet or dry at a specific time step, providing a constraint for estimating E_i. The mask takes a value of 0 during time steps when no E_i is simulated, and storage capacity S_v when E_i occurs. Since no observations of leaf water content are available at the sites, S_v is assumed to represent a wet canopy in the OSSE set-up. As microwave backscatter is sensitive to water content on the surface of the vegetation canopy, future research should focus on assimilating radar surface canopy water content estimates, in order to more accurately represent the short-term dynamics in E_i.

C. OSSE System Set-Up

In this study, 21 E experiments are conducted, including NR, CR, and four sets of assimilation runs. NR generates a "synthetic truth" and provides sub-daily pseudo-observations that mimic potential radar measurements. These pseudo-observations are later used in the assimilation runs to simulate the process of incorporating sub-daily radar observations into the E model. CR represents a traditional model run, which excludes these sub-daily radar observations and serves as a benchmark for the assimilation experiments. The assimilation runs use the pseudo-observations from NR to test the impact of prospective sub-daily radar observations on E modeling, comparing these results to the baseline performance of CR. The experiments aim to explore 1) the assimilation of sub-daily SSM to improve the estimation of E_t and E_b (SM3–SM24), 2) the use of sub-daily VOD for E_t modeling (V3–V12), and 3) the use of a wet/dry canopy mask as a constraint for E_i estimates (WD3–WD24). Moreover, a set of experiments combining the previous ones is executed (ALL3–ALL24). A summary of the experiments is provided in Table II, along with specificities about the experimental set-up and forcing data used in the experiments. The results of these experiments could serve as a basis for the determination of Level 2 SAR product accuracy requirements of future satellite missions studying short-term vegetation dynamics, like SLAINTE.

In NR, sub-daily GLEAM is executed with in situ measured forcing data at 3-hourly resolution, along with coarse-resolution (0.25°) SWE, high-resolution (0.1°) vegetation cover (MODIS/MEaSUREs) and high-resolution (250 m) soil properties (HiHydroSoil v2), and with the SSM and WDCS data assimilation switched off. NR yields 1) a time series of 3-hourly E estimates and its different components that can be contrasted against in situ latent heat flux measurements at the eddy-covariance sites to evaluate the actual skill of the sub-daily E model, 2) simulated SSM pseudo-observation time series that will be assimilated in further SM experiments, 3) a synthetic binary wet/dry canopy mask to constrain the wetness state of the canopy in the WD experiments, and 4) E pseudo-observations used to evaluate the other experiments, i.e., NR is defined as the "synthetic truth".

CR represents the current state-of-the-art in global E modeling. NR and CR use the same model configuration, i.e., sub-daily GLEAM, making this a twin experiment. Different meteorological forcing, and vegetation cover and soil properties are used, i.e., high spatial resolution data in NR, compared to coarse spatial resolution data in CR. In addition, sub-daily variations in VOD are not taken into account in CR. Instead, a constant daily VOD value is applied at every study site. In CR, ERA5 data at 3-hourly resolution are used as meteorological forcing, along with coarse-resolution vegetation data from MODIS/MEaSUREs and soil properties data from IGBP-DIS, both at 0.25° resolution. Due to uncertainties in the forcing data of CR, CR is expected to deviate from both the in situ latent heat flux and the E estimates obtained in NR. Given this additional uncertainty, CR can be used to demonstrate the added value of sub-daily SSM, sub-daily VOD, and the wet/dry canopy mask, derived from prospective sub-daily SAR data, to increase the accuracy in E modeling. In this regard, CR serves as a benchmark for comparing the SM, V, and WD experiments (see Table II) in terms of increase in performance against the synthetic truth (NR) for actual E, E_t, E_b, and E_i.

A total of 19 additional experiments are designed and executed to assess the impact of sub-daily SAR observations

of SSM, VOD, and WDCS, on E modeling over a range of climate regimes. The SM experiments focus on the assimilation of sub-daily SSM to improve the estimation of E_t and E_b. Time series of sub-daily SSM pseudo-observations are obtained from NR, to which an uncertainty of 4 vol% was added. ERA5 data are used as meteorological forcing and coarse-resolution soil properties and vegetation cover fractions are employed (0.25°). A Newtonian nudging algorithm based on SSM anomalies is used as the data assimilation approach [55], [74]:

$$w^+ = w^- + K\left(\hat{w}^0 - \hat{w}^-\right) \tag{1}$$

with w^+ the a posteriori SSM state, i.e., after application of the data assimilation, w^- the a priori SSM state, i.e., before the data assimilation, K the dimensionless nudging factor (quantifying the impact of the assimilation algorithm), $\hat{w}^0$ the pseudo-observed SSM anomaly, and $\hat{w}^-$ the modeled SSM anomaly. The SSM anomalies represent deviations relative to the monthly climatology of SSM. The monthly anomaly time series of the pseudo-observations (including uncertainty) are scaled toward the modeled SSM anomalies via cumulative density matching prior to assimilation in order to mitigate biases in the data assimilation system [55]. To account for sub-daily changes in the SSM climatology, the scaling of the complete time series is performed by first stratifying the observations by specific times of the day, and then individually scaling these to match the cumulative density function of the simulations corresponding to the same time of the day. This process is repeated for each subsequent time point. Once each subset of observations has been scaled using time-specific cumulative density matching, the scaled time series are recombined to form the complete, bias-corrected SSM anomaly time series. The nudging factor K is determined iteratively, whereby a value of 0.2 is found to give the best performance (not shown here). By assimilating every 3 (SM3), 6 (SM6), 9 (SM9), 12 (SM12), and 24 (SM24) hours, the impact of observation temporal frequency of potential future SAR missions is examined. In SM3, the synthetic observed SSM is assimilated every 3 hours (12 am, 3 am, 6 am, 9 am, 12 pm, 3 pm, 6 pm, 9 pm UTC), in SM6 every 6 hours (12 am, 6 am, 12 pm, 6 pm UTC), in SM9 every 9 hours (12 am, 9 am, 6 pm, 3 am, 12 pm, 9 pm, 6 am, 3 pm, etc. UTC), in SM12 every 12 hours (12 am, 12 pm UTC), and in SM24 every 24 hours (12 pm UTC).

The V experiments are designed to explore the value of sub-daily VOD to enhance E_t estimates. In total, four VOD experiments are conducted to assess the impact of the temporal resolution of these pseudo-observations. The SSM and WDCS data assimilation is deactivated for these experiments, allowing the model to operate in an open-loop configuration. ERA5 data are used as meteorological forcing, together with coarse-resolution vegetation cover fractions and soil properties (0.25°). Since VOD is a forcing variable in sub-daily GLEAM, rather than assimilated (contrary to SSM), a continuous 3-hourly VOD time series is required. VOD temporal resolutions of 3 (V3), 6 (V6), 9 (V9), and 12 (V12) hours are evaluated. For coarser resolutions (V6, V9, V12), the VOD value from the most recent defined timestep is retained until the next defined timestep, ensuring a continuous 3-hourly time series.

Moreover, as SAR observations can inform about the wetness state of the canopy, five experiments, focusing on the role of SAR observations of WDCS in improving E_i estimates (WD), are conducted. The binary mask is created based on E_i time series from NR, taking a value of 0 during time steps when no E_i is estimated, and storage capacity S_v when E_i takes place. A 5% misclassification is incorporated in the time series to account for the accuracy level of the prospective SAR retrievals. This misclassification involves randomly altering an equal number of observations from 0 to S_v and from S_v to 0. A data assimilation scheme using this binary mask is then implemented in the sub-daily E_i module to update the canopy storage following a Newtonian nudging approach:

$$C_v^+ = C_v^- + K\left(C_v^0 - C_v^-\right) \tag{2}$$

where C_v^+ is the a posteriori canopy storage state, i.e., after application of the data assimilation, C_v^- is the a priori canopy storage state, i.e., before the data assimilation, and C_v^0 is the pseudo-observed binary WDCS, taking the value 0 or storage capacity S_v. A nudging factor K of 0.5 was assumed, and the assimilation is applied only at times when the mask implies there is water present on the canopy, but the modeled canopy storage is zero, or the other way around. The assimilation is conducted in only these two specific scenarios because the data assimilation of WDCS concentrates on detecting the presence or absence of water on the canopy, rather than on quantifying the exact amount of water present. The observation temporal frequency of this binary data assimilation system is studied by assimilating the mask every 3 (WD3), 6 (WD6), 9 (WD9), 12 (WD12), and 24 (WD24) hours. In these WD experiments, sub-daily GLEAM is forced with ERA5 meteorological data, coarse-resolution (0.25°) soil properties and vegetation cover fractions. In addition, different misclassification levels are studied, and the impact of using a nudging factor K of 1 is tested.

Finally, to fully exploit the potential of a sub-daily SAR satellite constellation, all prospective sub-daily SAR observations are combined in a final OSSE set (ALL). This includes the assimilation of sub-daily SSM, the binary assimilation of sub-daily WDCS, and the use of sub-daily VOD as forcing. This is performed for different temporal frequencies, i.e., 3 (ALL3), 6 (ALL6), 9 (ALL9), 12 (ALL12) and 24 (ALL24) hours. For this experiment, ERA5 data are used as meteorological forcing, together with coarse-resolution (0.25°) vegetation cover fractions and soil properties in the sub-daily E model.

IV. Results

A. NR and CR Validation

To evaluate the actual skill of the sub-daily E model, the simulated E estimates from NR should be close to the real observations of E at the eddy-covariance sites. Therefore, the NR simulations are first validated against the measured latent heat flux (converted to E values using the latent heat of vaporization of water) at the four forest study sites; see Fig. 4. Results indicate that sub-daily GLEAM is able to capture and represent the daily cycle of E across all study sites, with better results obtained in summer (JJA) when maximum E and its diurnal amplitude are the highest, with a correlation coefficient exceeding 0.7 for all sites. The model is performing worse at FR-Pue in JJA, with a general overestimation, and relatively high RMSE of 0.247 mm/3 hours. During winter months (DJF),

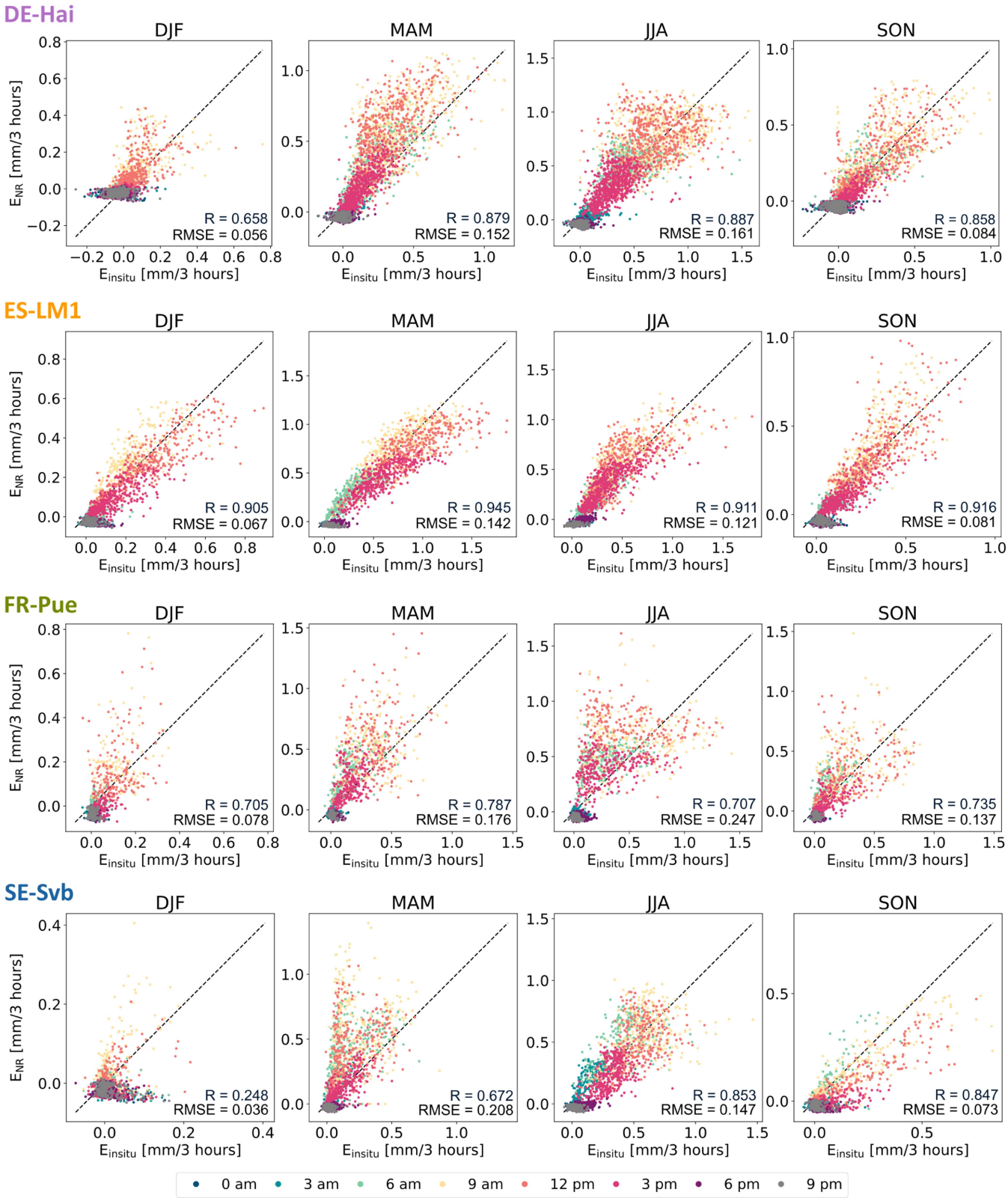

Fig. 4. Scatterplots of E [mm/3 hours] modeled by sub-daily GLEAM in NR (E_{NR}) in function of in situ measured E (E_{insitu}) at the four eddy-covariance forest sites, for winter (DJF), spring (MAM), summer (JJA), and autumn (SON). Pearson correlation coefficient (R) and Root-Mean-Square-Error (RMSE) in mm/3 hours are reported.

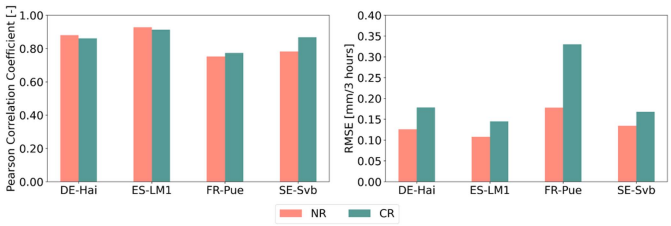

Fig. 5. Pearson correlation coefficient (left) and RMSE (right) for NR and CR compared to in situ latent heat flux values [W/m^2], converted to E [mm/3 hours], measured at the four eddy-covariance forest sites.

the model overestimates E in the morning (9 am) and noon (12 pm), except for ES-LM1, where higher values of E are observed compared to other sites.

Additionally, the skill of CR is evaluated, which is expected to perform worse than NR when compared to in situ measurements because of the use of coarser resolution forcing data representing the benchmark for the assimilation experiments. Fig. 5 shows the Pearson correlation coefficient (left) and RMSE (right) for NR and CR compared to in situ E observations, at the four forest study sites. In terms of correlation, the performance of NR and CR is similar, with higher correlation for NR observed for DE-Hai and ES-LM1, and lower correlation for FR-Pue and SE-Svb. For RMSE, the difference in performance is more clear with higher RMSE for CR compared to NR, illustrating that CR is performing overall worse than NR. Furthermore, CR is evaluated against NR in terms of Nash-Sutcliffe Efficiency (NSE) (not shown here). The lowest NSE is observed for FR-Pue, with an NSE value of 0.04, followed by SE-Svb (0.54), ES-LM1 (0.70), and the highest NSE is found for DE-Hai (0.74), illustrating a good skill of the CR model set-up. Consequently, CR can serve as a benchmark to evaluate the potential of sub-daily SAR (pseudo-)observations to bring CR closer to the synthetic truth represented by NR. This is explored in further experiments whose results are reported in the following sections.

B. Sub-Daily SSM

Fig. 6 summarizes Taylor diagrams of the SM, V, and WD experiments (see Section III). The colors correspond to the different sites, as shown in Fig. 2, and the shape of the points indicates the temporal frequency. The radial distance from the origin represents the normalized standard deviation. The correlation coefficient is indicated by the azimuthal angle, and normalized RMSE is indicated by the radial lines. Overall, better performance is indicated by a shorter distance to the red star, i.e., reference point, that marks the synthetic truth coming from NR. The top row shows summary results of the influence of assimilating sub-daily SSM with different temporal resolutions. Results are presented for SSM and E. The Taylor diagrams reveal that assimilating synthetic sub-daily SSM slightly improves SSM estimates in SE-Svb and FR-Pue, mainly in terms of reduction in normalized standard deviation. Only a limited impact is observed in DE-Hai and ES-LM1. There is no visible impact on the E estimates, and this applies to all sites. In addition to the Taylor diagrams, which provide an overall assessment of performance across all sites and temporal frequencies, Fig. 7 presents the percentage improvement of each experiment relative to CR, i.e., the baseline state-of-the-art in E modeling, expressed as ΔRMSE (%). Here, ΔRMSE is computed as

$$\Delta\text{RMSE} = \frac{\text{RMSE}_{\text{CR}} - \text{RMSE}_{\text{exp}}}{\text{RMSE}_{\text{CR}}} \tag{3}$$

with RMSE_{CR} the RMSE of CR against NR, and RMSE_{exp} the RMSE of each experiment against NR. To highlight seasonal differences, three temporal subsets are considered: all days of the year (ALL YEAR), the winter months December–January–February (DJF), and the summer months July–August–September (JJA). Only limited improvements in SSM are obtained for the SM experiments when all days of the year are considered, with ΔRMSE values up to 4%. The largest relative improvement is found at DE-Hai during summer, particularly when assimilating observations at a 3-hourly resolution, although the overall improvement remains modest (up to 9.32%). Negative ΔRMSE values are observed for SE-Svb in winter, and for ES-LM1 in both winter and summer. Regarding the impact on total E, the SM experiments generally lead to negative ΔRMSE values, with the strongest degradations occurring at ES-LM1, especially during summer.

C. Sub-Daily VOD

The V experiments indicate that, when available at sub-daily resolutions, VOD is an effective constraint for plant water stress that can substantially improve E_{t} and E estimates (Fig. 6, middle row). The daily constraint, represented by CR, is noticeably less valuable compared to sub-daily constraints. The availability of VOD data twice a day (V12) can already improve the skill of the E model. As the temporal resolution increases, the modeling results improve, especially in terms of a decrease in normalized RMSE and normalized standard deviation. Overall, good results are obtained with a temporal resolution of 6 hours at 6 am, 12 pm, 6 pm, and 12 am (V6), including the midday peak of water stress. The ΔRMSE in Fig. 7 for E_{t} highlights the importance of having VOD observations available around midday, when plant water stress is highest and E reaches its maximum. When all days of the year are considered, implementing VOD twice per day (V12), including midday, leads to substantial improvements, with ΔRMSE values of 17%, 32%, 31%, and 28% for DE-Hai, ES-LM1, FR-Pue, and SE-Svb, respectively. Increasing the temporal resolution to V6 further enhances performance at most sites, except for DE-Hai, where improvements remain similar to V12. At the highest temporal resolution (V3), performance decreases relative to V12 and V6 for DE-Hai and ES-LM1, but continues to increase for FR-Pue and SE-Svb. Seasonal results show that the benefit of using sub-daily VOD varies across sites: FR-Pue consistently benefits throughout the year, DE-Hai and ES-LM1 show the largest gains in winter, while SE-Svb exhibits the strongest improvements in summer. Given the strong influence of E_{t} on total E in forests, similar patterns in ΔRMSE are observed when evaluating the impact on overall E.

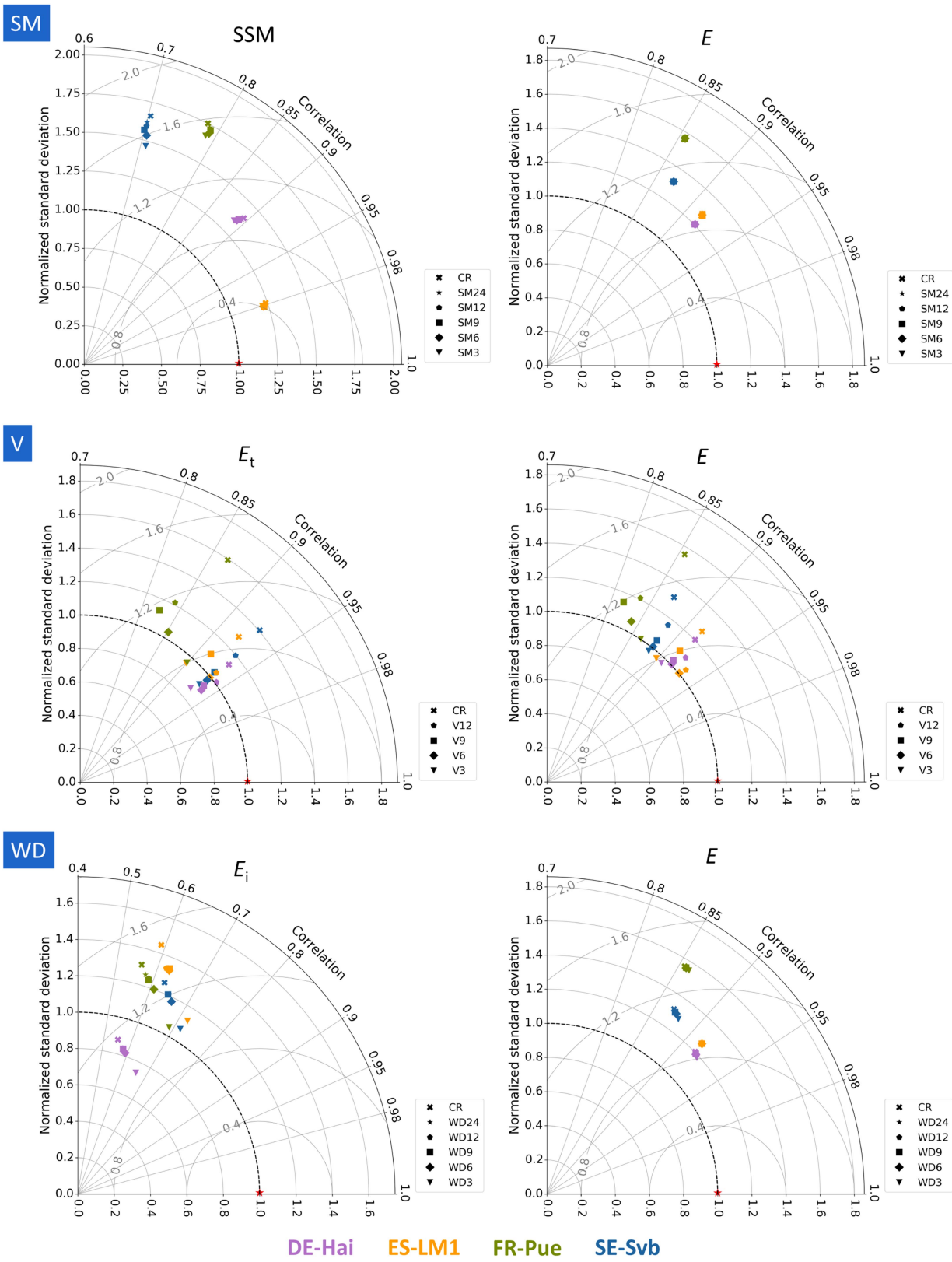

Fig. 6. Taylor diagrams summarizing the E experiments. The top figures indicate the influence of assimilating SSM with different temporal resolutions on sub-daily GLEAM SSM (left) and E (right). The middle figures show the result of using VOD with different temporal resolutions and the influence it has on E_t (left) and E (right). The influence of constraining the canopy storage with WDCS observations is shown on the bottom, both for E_i (left) as well as E (right). Colors are used to indicate the specific sites, i.e., Hainich (DE-Hai), Majadas del Tiétar North (ES-LM1), Puéchabon (FR-Pue), or Svartberget (SE-Svb).

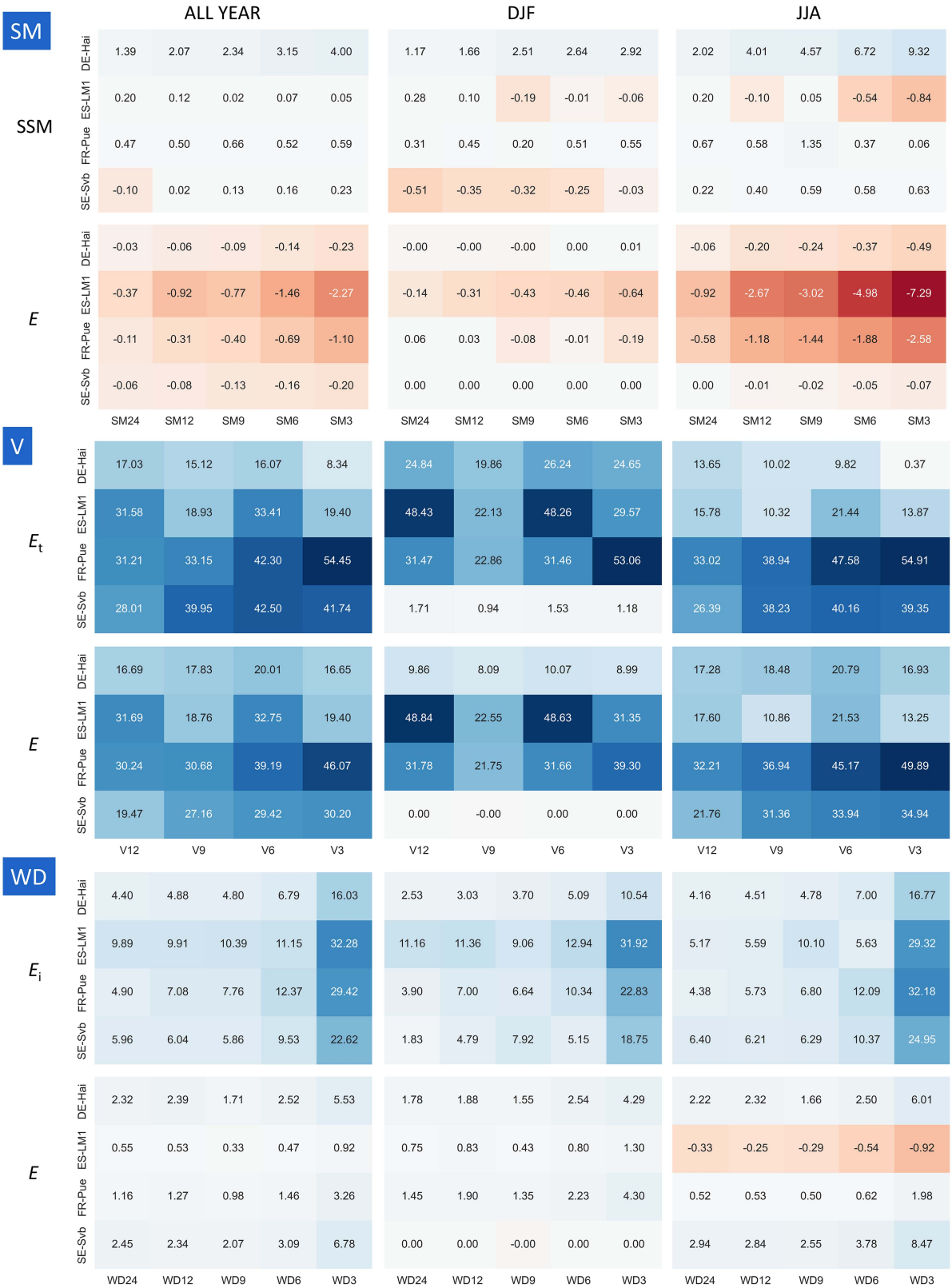

Fig. 7. Relative improvement in model performance of the sub-daily experiments compared to CR, expressed as ΔRMSE (%), for three temporal subsets: all days of the year (ALL YEAR; left column), winter months December–January–February (DJF; middle column), summer months July–August–September (JJA; right column). The top figures (SM) indicate the influence of assimilating SSM with different temporal resolutions on sub-daily GLEAM SSM and E. The middle figures (V) show the result of using VOD with different temporal resolutions and the influence it has on E_t and E. The influence of constraining the canopy storage with WDCS observations is shown on the bottom (WD), both for E_i as well as E. Blue-toned colors represent an increase in model performance (positive ΔRMSE), and red-toned colors represent a decrease in model performance (negative ΔRMSE).

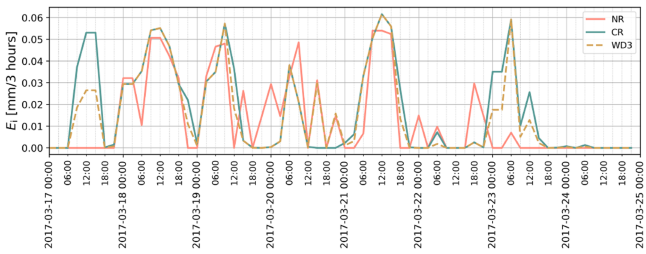

Fig. 8. Example time series of E_i estimates at the site in Germany (DE-Hai), for the period 17 March 2017 until 25 March 2017 for NR, CR, and WD3.

D. Sub-Daily WDCS

To illustrate the impact of the data assimilation system with binary WDCS (pseudo-)observations, time series of E_i estimates are shown in Fig. 8 for NR, CR, and WD3 for the site DE-Hai, as an example. On March 17, no E_i is simulated by NR, while for CR, E_i estimates up to 0.05 mm/3 hours occur. In the WD3 experiment, the impact of the binary mask results in a reduction of the E_i estimates, as a result of assimilating a dry canopy state during this day. On the other hand, in the afternoon and evening of March 20, CR simulates no E_i, while NR does. In this case, the canopy storage is updated in WD3 by assimilating a wet canopy observation (interpreted as saturated canopy storage), implying there is water available on the canopy that can evaporate. At times when both CR and NR simulate E_i, no data assimilation is applied, resulting in the same E_i estimates for CR and WD3 (e.g., on March 18). Likewise, at times when no E_i is simulated in NR and CR, no data assimilation is applied in WD3 implying that there is no E_i simulated (e.g. afternoon/evening on March 24), unless adjusted based on the introduced misclassification. Overall, the time series indicate that the binary WDCS mask is a useful constraint to improve E_i estimates in sub-daily GLEAM, whereby the focus is on the detection of E_i events, rather than on the exact amount of water that is intercepted. As this research study is the first one assessing the potential of SAR observations to constrain E_i estimates, further research is needed to develop retrieval algorithms for WDCS observations from microwave data. However, this is beyond the scope of this study.

Fig. 9 illustrates the impact of the nudging factor used in the data assimilation of binary WDCS observations and the effect of different detection accuracy levels in this binary time series (no, 5%, 10%, 20%, and 40% misclassification). The left Taylor diagram shows the result for a nudging factor of 0.5 and the right one for a nudging factor of 1. The best assimilation results, mainly in terms of highest correlation and lowest normalized RMSE, are obtained when a nudging factor of 1 is applied and no misclassification is introduced in the observation time series (corresponding with a perfect accuracy of the satellite product). When a perfect accuracy satellite product is available, the gain of assimilating is lower for a nudging factor of 0.5 compared to 1. However, when the quality of the satellite products reduces (higher misclassification levels), the performance strongly decreases for a nudging factor of 1. While for a nudging factor of 0.5, the decrease in performance, when moving toward less accurate satellite products, is smaller. In addition, the results show that at least a detection accuracy of 90% (corresponding to a 10% misclassification) is needed in order to improve E_i estimates, given ERA5 data as forcing in the E model. Therefore, a misclassification level of 5%, corresponding to a detection accuracy of 95%, and a nudging factor of 0.5 is selected to perform the final WD experiments in this study.

The Taylor diagrams in Fig. 6 reveal that the use of a wet/dry canopy mask as a constraint to improve E_i estimates is valuable at all four sites, with the strongest increase in performance observed when a temporal resolution of 3 hours (WD3) is considered. For DE-Hai and FR-Pue, the correlation increases from ∼0.55 to 0.66 for DE-Hai and towards 0.69 for FR-Pue. The highest correlation is found for SE-Svb and ES-LM1 (an increase in correlation from ∼0.6 to 0.72). The plots show a strong reduction in normalized RMSE for WD3 compared to CR for all sites. In terms of normalized standard deviation, better results are observed for ES-LM1, FR-Pue, and SE-Svb for which the normalized standard deviation is close to 1, implying that the standard deviation of the experimental results is similar to the one of NR. For DE-Hai, the normalized standard deviation is smaller than 1, illustrating that the standard deviation of the WD output for this site is smaller than the one for NR. Fig. 7 also shows that assimilating WDCS at a 3-hourly interval yields the largest improvements, with the strongest gains observed for ES-LM1 and FR-Pue (ΔRMSE of 32% and 29% respectively, when considering the full year). Seasonal variations in performance are relatively limited, and assimilation every 3 hours consistently provides the best results across all sites, with an average ΔRMSE of 21% in winter and 26% in summer. In terms of total E, the impact of assimilating WDCS observations is less pronounced.

E. Combined Impact of Sub-Daily Microwave Observations

The combined impact of synthetic sub-daily microwave observations, i.e., SSM, VOD, and WDCS, in constraining total E estimates, is shown in Fig. 10. Constraining the sub-daily E model with daily and twice-daily microwave observations does not strongly improve E estimates. The best performance is observed with a temporal resolution of 6 hours (12 am, 6 am, 12 pm and 6 pm), including observations during water-stressed times of the day, and corresponding to the optimal resolution of the VOD experiments. This is because VOD impacts E_t which is the largest component of E in all four sites. The best results are observed for ES-LM1, where times with water stress are more common. At this site, the normalized standard deviation reduces from 1.26 to 0.92 from daily (ALL24) to 6-hourly observations (ALL6), and correlation increases from 0.92 to 0.94 for E.

V. Discussion

This study focuses on forest sites in Europe. Previous work by Chen et al. [75] shows that footprint-related uncertainty strongly depends on the degree of spatial heterogeneity surrounding eddy-covariance towers. To minimize this effect, we selected forest sites located within homogeneous forested landscapes. Additionally, a quality assessment of several European eddy-covariance sites, including Hainich, Majadas del Tiétar, and Puéchabon, conducted by Göckede et al. [76] demonstrated

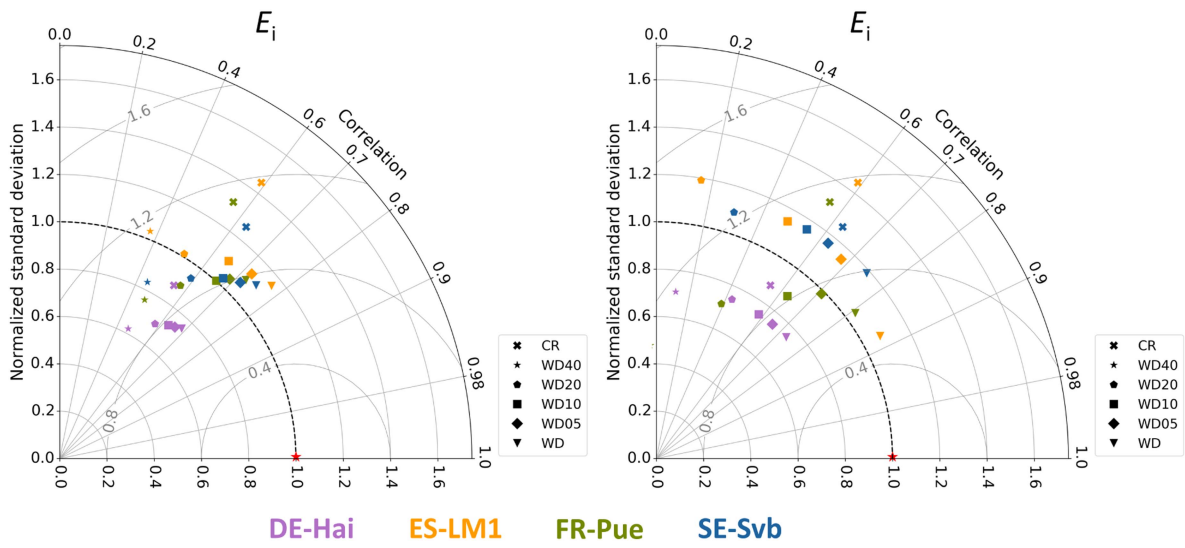

Fig. 9. Taylor diagrams summarizing the impact of the nudging factor (equal to 0.5 on the left figure and 1 on the right) and misclassification levels (WD05: 5%, WD10: 10%, WD20: 20%, and WD40: 40% misclassification of binary values) on E_i estimates for the WD experiments. The results shown here represent the impact of the data assimilation of the WDCS observations every 3 hours. Colors are used to indicate the specific sites, i.e., Hainich (DE-Hai), Majadas del Tiétar North (ES-LM1), Puéchabon (FR-Pue), or Svartberget (SE-Svb).

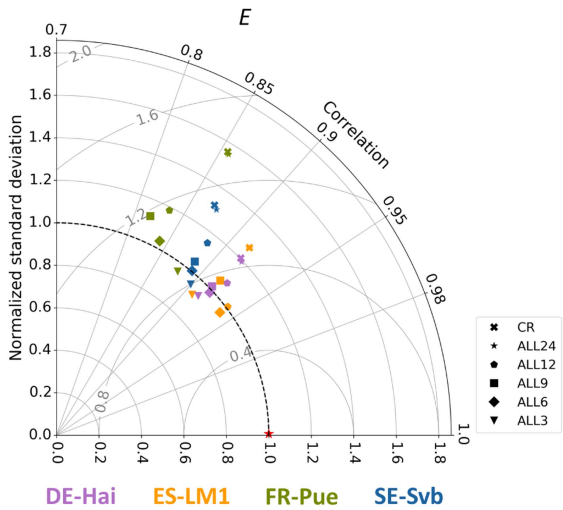

Fig. 10. Taylor diagram summarizing the combined E experiments (ALL). The figure indicates the combined impact of assimilating SSM, the use of sub-daily VOD, and the binary assimilation of WDCS observations on total E estimates, for different temporal resolutions. Colors are used to indicate the specific sites, i.e., Hainich (DE-Hai), Las Majadas del Tiétar North (ES-LM1), Puéchabon (FR-Pue), or Svartberget (SE-Svb).

that these towers accurately represent their respective forest land cover types and do not require footprint corrections. This provides confidence that the selected sites are appropriate for our analysis and are not substantially affected by footprint-induced biases. A related consideration is the well-known lack of energy balance closure at eddy-covariance sites. Studies, such as those by Mauder et al. [77] and Zhang et al. [78], report a systematic imbalance of approximately 20%, leading to an underestimation of latent heat flux. While this source of uncertainty affects the absolute magnitude of the fluxes, it does not influence the central aim of our study, which focuses on the relative improvement achieved through assimilating sub-daily SAR observations rather than on the absolute accuracy of the final estimates. Additional studies are recommended in other biomes to explore the sensitivity of sub-daily GLEAM and the value of the sub-daily observations in a wider range of vegetation types (e.g., farmland, grasslands) and climate zones (e.g., tropical and arid regions).

A Priestley and Taylor formulation is adopted in this study to estimate potential evaporation, as previous work has shown that radiation-driven approaches tend to outperform more complex Penman-based approaches at the ecosystem scale [79], [80]. Penman-based methods require a larger number of input variables, which increases the overall uncertainty, particularly due to the limited availability and quality of canopy and aerodynamic conductance estimates. In addition, Penman–Monteith approaches would require dynamically resolving stomatal conductance at sub-daily time scales, a process that, despite its relevance when moving toward high temporal resolution, remains highly uncertain at sub-daily scales [79]. The Priestley and Taylor approach therefore offers a more robust and reliable option for the sub-daily framework in this study. In the applied Priestley and Taylor approach, the α factor represents the aerodynamic term as a factor of the radiation component. As the radiation component varies throughout the day by relying on sub-daily forcing data, sub-daily variability is also represented in aerodynamic processes. In addition, to properly represent nighttime conditions, a correction is applied for periods when potential evaporation becomes negative (i.e., condensation), removing the radiative component and retaining only the aerodynamic term [55]. In addition, land-cover-specific α coefficients are used following Martens et al. [55]. Given that E is computed as the product of sub-daily S, representing the moisture stress constraint originating from both the soil and the vegetation, and the potential evaporation, the Priestley and Taylor approach can be considered as a robust and suitable method for estimating sub-daily E and its components.

The results of this study indicate an overall good performance of the sub-daily E model, particularly during the summer months. In winter, however, the model tends to overestimate early-morning E, especially at DE-Hai, FR-Pue, and SE-Svb. Given that SE-Svb and DE-Hai perform well in summer, the reduced skill in winter is likely related to the presence of snow, suggesting that sub-daily GLEAM is not able to fully capture snow-related processes. FR-Pue shows somewhat lower performance across all seasons, which may be attributed to uncertainties in the vegetation and soil property datasets used in the NR simulation. Although these datasets are relatively high resolution, they may still not fully represent the tower footprint. Nonetheless, due to the homogeneous forest cover at the sites, any resulting mismatch is expected to be limited. Additional inaccuracies may arise from the dynamic forcing data, including the synthetically generated sub-daily VOD time series. The use of synthetically generated sub-daily VOD data based on latent heat flux observations is a strong assumption in this manuscript. However, this approach represents the most feasible option at present, as no real sub-daily VOD observations are currently available. Confidence in this assumption is supported by studies demonstrating strong relationships between landscape-scale satellite-derived VOD and plant-scale physiological metrics [30], [71], [72]. Future research using real sub-daily VOD observations (e.g., from GNSS, GNSS-R, or field campaign data) may offer the first practical means of incorporating real sub-daily VOD observations into E models [81]. Inaccuracies in the model framework might be an additional source of error. For instance, an overestimation of E at FR-Pue has previously been reported for the daily version of GLEAM as well [82]. Moreover, the results suggest that sub-daily GLEAM does not fully capture the rapid dry-out characteristic of this Mediterranean site during summer (not shown here), which likely contributes further to the observed overestimation. Despite these sources of uncertainty, the results provide confidence in the ability of sub-daily GLEAM to capture the diurnal variability in E. This supports its suitability for evaluating the potential impact of sub-daily SAR observations, and therefore justifies the use of the NR simulations as the synthetic truth in the subsequent experiments.

The results of the SM experiments show no substantial improvement in performance when assimilating SSM observations, compared to CR where no SSM was assimilated. The reason for this might be that the effect of SSM on E is concentrated only in periods of water limitation and vegetation stress. In DE-Hai and SE-Svb, water availability is seldom limiting E, and for FR-Pue and ES-LM1 only during part of the year. Moreover, the ERA5 forcing data generally display a high performance at the sites, as seen in comparisons against in situ data (see Fig. 5). Generally, SSM data assimilation is expected to have a strong impact in correcting missing precipitation events. Since the ERA5 meteorological data used for these experiments are already very accurate, the assimilation of SSM is not bringing the results significantly closer to NR. In addition to the generally good quality of the ERA5 meteorological forcing, it is important to highlight the role of observational noise. The noise added to the NR SSM output, representing pseudo-observations in the assimilation experiments, follows a normal distribution with mean 0 and a standard deviation of 4 vol%. This uncertainty is relatively high compared to the actual diurnal range of SSM observed at the forest sites. Specifically, the average diurnal SSM range is approximately 0.7 vol% for DE-Hai, 1 vol% for ES-LM1, 1.3 vol% for FR-Pue, and 0.7 vol% for SE-Svb, meaning that the assumed 4 vol% exceeds the natural diurnal variability. Nevertheless, this value reflects the threshold measurement uncertainty target for satellite-based SSM retrievals according to GCOS, and was therefore used as a realistic benchmark for our OSSE setup. For ES-LM1, the reduced performance in summer can be attributed to the site's climate, where rainfall is scarce and highly episodic, especially in summer. Under these conditions, the impact of assimilating SSM becomes larger because of the limited diurnal variability in soil moisture, while the added noise in the pseudo-observations dominates the signal. As a result, SSM assimilation may degrade the model state rather than improve it, leading to lower ΔRMSE values. This negative effect on SSM propagates to the E estimates, producing the strongly negative values observed for ES-LM1 in summer. The lower performance at SE-Svb during winter is likely related to snow presence at the site.

Regarding the V experiments, the results indicate that assimilating VOD four times per day (V6) leads to substantial improvements in estimating E with an average ΔRMSE value of around 30% across all four sites. This suggests that incorporating VOD observations at multiple times per day provides a stronger constraint on E_t than daily or twice-daily observations. These findings, however, are conditioned on the empirical way VOD is used within sub-daily GLEAM and are therefore model-dependent. Furthermore, the results show that implementing VOD at a 3-hourly frequency (V3) does not consistently lead to better performance compared to 6-hourly (V6) or 12-hourly (V12) implementation. Theoretically, one would expect the highest temporal resolution to yield the best performance; however, the uncertainty inherent in the synthetically generated VOD time series may limit the benefit of V3. Future research using real sub-daily VOD observations (e.g., from GNSS, GNSS-R, or field campaign data) may help clarify the potential added value of higher temporal sampling.

In terms of temporal resolution of WDCS observations, one can conclude that information about the wetness state of the canopy is most useful at high temporal resolution (WD3), as it provides the best opportunity to capture precipitation events. As the temporal frequency of the observations decreases, the observation constraint becomes less valuable. This is the case for all studied sites. Yet, even when only one observation per day is applied (WD24), the performance is still better compared to no constraint at all (CR). An observation every 6 hours, corresponding with the proposed acquisition timing of SLAINTE, clearly improves the E_i estimates compared to daily observations. The strongest improvements are observed at the Mediterranean sites ES-LM1 and FR-Pue. This can be attributed to the characteristic rainfall regime of Mediterranean climates, where long dry periods are punctuated by short, intense rainfall events, particularly during summer. Under such conditions, updating canopy storage is expected to substantially improve E_i estimates, especially during rainfall events that the CR does not always capture accurately in timing. The low impact of assimilating WDCS observations to E estimates is expected,

as the contribution of E_i to total E is small, compared with that of E_t, making improvements in canopy wetness state less visible in the total E signal.

Both sub-daily VOD and WDCS observations exhibit the strongest impact on improving E estimates. When all sub-daily observations are considered together, the largest combined improvement is obtained when using 6-hourly observations (12 am, 6 am, 12 pm, and 6 pm). Lower temporal resolutions perform substantially worse, suggesting they miss key moments of plant water stress during the day as well as rainfall interception events, leading to a less accurate representation of the diurnal cycle of E. These findings are in line with Holtzman et al. [51], where an observation frequency of four times per day was found to be sufficient to capture the diurnal amplitude of leaf water potential, resulting in an increased accuracy in estimating E, compared to daily or twice-daily observations. Moreover, they report that the accuracy found with an observation frequency of four times per day, including midnight, predawn, midday, and dusk, is similar to the one obtained when hourly observations are considered, illustrating that those observation timings are crucial in monitoring daily cycles of moisture redistribution within the soil–plant–atmosphere continuum. Furthermore, Schackow et al. [83] studied the diurnal hysteresis of sap flow data in function of VPD and demonstrated how these hysteresis patterns reveal different levels of plant hydraulic stress across a wide range of biomes using in situ sap flow data. Because sap flow is linked to changes in canopy water content, high temporal resolution information on vegetation water status can be used to identify early signs of vegetation stress. They determined the minimum sub-daily observation frequency required to capture this diurnal hysteresis using microwave remote sensing. Their findings indicate that at least three overpasses per day, specifically at 6 am, 12 pm, and 6 pm (excluding the midnight overpass) are needed to adequately characterize the diurnal sap flow hysteresis and monitor vegetation health. This minimum 6-hourly sampling interval aligns with our results on VOD temporal frequency, where 6-hourly temporal resolution, including 6 am, 12 pm, and 6 pm, yields substantially better estimation performance than daily (12 pm) or twice-daily (12 am and 12 pm) observations.

VI. Conclusion

The capability of sub-daily microwave remote sensing to monitor diurnal variations in soil moisture and vegetation water content presents a significant opportunity to observe the short-term dynamics of Earth's ecosystems. Such observations are particularly pertinent in the context of our changing climate, offering insight into the daily cycles of different states and fluxes, which can be indicative of the functional health of ecosystems. Diurnal fluctuations in vegetation water content are key in driving rapid land–atmosphere interactions, primarily through their connection to the partitioning of available energy into latent and sensible heat fluxes. This study investigates the value of prospective sub-daily microwave observations specifically for the modeling of E in forests. It does so by evaluating the potential of sub-daily retrievals of SSM, VOD, and WDCS to enhance our understanding of these complex processes at four European forest sites.

The experiments demonstrate that sub-daily observations of SSM, VOD, and WDCS can be ingested in current-generation E models (e.g., GLEAM) to provide constraints on E estimates and its main components (E_b, E_t and E_i). The results show that a WDCS observation with a temporal resolution of 3 hours is a valuable constraint to improve E_i estimates, and the impact is observed over all study sites and all seasons. However, the influence of uncertainties in this WDCS should be further investigated in future work. Furthermore, the experiments indicate that, when available at sub-daily resolutions, VOD is an effective constraint for plant water stress that can substantially improve E_t estimates. The best results are observed when VOD is incorporated four times a day, i.e., a temporal resolution of 6 hours (12 am, 6 am, 12 pm, and 6 pm), compared to daily or twice-daily observations. The effect of assimilating sub-daily SSM on E is concentrated in periods of water limitation, and mainly affects E_b estimates. However, because of the high quality of current precipitation forcing datasets (e.g., ERA5), and the large uncertainty level in our synthetic SSM observations, compared to their diurnal amplitude, assimilating sub-daily SSM does not lead to improvements in E estimates, even under conditions of vegetation water stress. Overall, the added value of incorporating sub-daily SAR observations in E modeling becomes particularly evident when observations are taken every 6 hours, at predawn (6 am UTC), midday (12 pm UTC), dusk (6 pm UTC), and midnight (12 am UTC), compared to daily (12 pm UTC) or twice-daily (12 am and 12 pm UTC) observations. This frequency allows for detailed monitoring of the diurnal variations in soil and vegetation water content, thereby enabling the identification of critical periods such as those of water stress.

This investigation encompasses specific assumptions and limitations that should be acknowledged. First, the analysis relies solely on a single model, i.e., sub-daily GLEAM, rendering the outcomes potentially model-specific. Since no alternative E models are currently available that allow the ingestion of sub-daily microwave retrievals to assess their potential value in E monitoring, GLEAM is selected in this study because of its high reliance on microwave data. Future research might explore the utility of alternative E models. Furthermore, the study's scope is confined to four forest sites, all located in Europe, thus addressing a restricted range of climatic conditions. Given these constraints, future research efforts should focus on expanding the application of the proposed methodology across a broader range of locations, encompassing diverse vegetation types and climatic conditions. In addition, the conclusions drawn from this study are based on synthetic observations, including SSM, VOD, and WDCS. The initiation of field campaigns, integrating sub-daily radar observations with co-located in situ measurements of relevant geophysical variables, would significantly contribute to elucidating the value and applicability of sub-daily SAR data in the context of E modeling. The findings of this research highlight the critical role of initiatives such as the SLAINTE mission idea in deepening our understanding of hydrological short-term dynamics within ecosystems. By leveraging such high-resolution temporal data, the scientific community can gain unprecedented insights into the diurnal patterns of water exchange, thereby facilitating a more nuanced comprehension of ecosystem responses to environmental stress.

REFERENCES

[1] J. L. Monteith, "Evaporation and Environment," in *Symposia of the Society for Experimental Biology*, vol. 19. Cambridge, MA, USA: Cambridge Univ. Press, 1965, pp. 205–234.

[2] L. Gimeno, A. Drumond, R. Nieto, R. M. Trigo, and A. Stohl, "On the origin of continental precipitation," *Geophysical Res. Lett.*, vol. 37, no. 13, 2010, Art. no. L13804.

[3] W. Dorigo et al., "Closing the water cycle from observations across scales: Where do we stand?," *Bull. Amer. Meteorological Soc.*, vol. 102, no. 10, pp. E1897–E1935, 2021.

[4] D. G. Miralles et al., "The WACMOS-ET project–Part 2: Evaluation of global terrestrial evaporation data sets," *Hydrol. Earth System Sci.*, vol. 20, no. 2, pp. 823–842, 2016.

[5] C. J. Talsma et al., "Partitioning of evapotranspiration in remote sensing-based models," *Agricultural Forest Meteorol.*, vol. 260, pp. 131–143, 2018.

[6] Y. Zhang et al., "Multi-decadal trends in global terrestrial evapotranspiration and its components," *Sci. Rep.*, vol. 6, no. 1, 2016, Art. no. 19124.

[7] S. T. Allen et al., "Key questions on the evaporation and transport of intercepted precipitation," in *Precipitation Partitioning by Vegetation: A Global Synthesis*, J. T. Van Stan II, E. Gutmann, and J. Friesen, Eds. Berlin, Germany: Springer International Publishing, 2020, pp. 269–280.

[8] J. Blunden, T. Boyer, and E. Bartow-Gillies, "State of the climate in 2022," *Bull. Amer. Meteorological Soc.*, vol. 104, no. 9, pp. Si–S501, 2023.

[9] D. G. Miralles et al., "El Niño–La Niña cycle and recent trends in continental evaporation," *Nature Climate Change*, vol. 4, no. 2, pp. 122–126, 2014.

[10] W. Brutsaert, "Global land surface evaporation trend during the past half century: Corroboration by Clausius-Clapeyron scaling," *Adv. Water Resour.*, vol. 106, pp. 3–5, 2017.

[11] Y. Yang et al., "Evapotranspiration on a greening earth," *Nature Rev. Earth Environ.*, vol. 4, no. 9, pp. 626–641, 2023.

[12] A. J. Teuling et al., "A regional perspective on trends in continental evaporation," *Geophysical Res. Lett.*, vol. 36, no. 2, 2009, Art. no. L02404.

[13] P. C. D. Milly and K. A. Dunne, "Potential evapotranspiration and continental drying," *Nature Climate Change*, vol. 6, no. 10, pp. 946–949, 2016.

[14] P. C. D. Milly, K. A. Dunne, and A. V. Vecchia, "Global pattern of trends in streamflow and water availability in a changing climate," *Nature*, vol. 438, no. 7066, pp. 347–350, 2005.

[15] M. Rahmati et al., "Continuous increase in evaporative demand shortened the growing season of European ecosystems in the last decade," *Commun. Earth Environ.*, vol. 4, no. 1, 2023, Art. no. 236.

[16] D. G. Miralles, P. Gentine, S. I. Seneviratne, and A. J. Teuling, "Land–atmospheric feedbacks during droughts and heatwaves: State of the science and current challenges," *Ann. New York Acad. Sci.*, vol. 1436, no. 1, pp. 19–35, 2019.

[17] J. B. Fisher et al., "The future of evapotranspiration: Global requirements for ecosystem functioning, carbon and climate feedbacks, agricultural management, and water resources," *Water Resour. Res.*, vol. 53, no. 4, pp. 2618–2626, 2017.

[18] J. Vilà-Guerau de Arellano et al., "Advancing understanding of land–atmosphere interactions by breaking discipline and scale barriers," *Ann. New York Acad. Sci.*, vol. 1522, no. 1, pp. 74–97, 2023.

[19] G. B. Bonan, "Forests and climate change: Forcings, feedbacks, and the climate benefits of forests," *Science*, vol. 320, no. 5882, pp. 1444–1449, 2008.

[20] M. F. McCabe et al., "The future of Earth observation in hydrology," *Hydrol. Earth System Sci.*, vol. 21, no. 7, pp. 3879–3914, 2017.

[21] J. D. Kalma, T. R. McVicar, and M. F. McCabe, "Estimating land surface evaporation: A review of methods using remotely sensed surface temperature data," *Surv. Geophys.*, vol. 29, pp. 421–469, 2008.

[22] K. Wang and R. E. Dickinson, "A review of global terrestrial evapotranspiration: Observation, modeling, climatology, and climatic variability," *Rev. Geophys.*, vol. 50, no. 2, 2012, Art. no. RG2005.

[23] J. B. Fisher et al., "ECOSTRESS: NASA's next generation mission to measure evapotranspiration from the International Space Station," *Water Resour. Res.*, vol. 56, no. 4, 2020, Art. no. e2019WR026058.

[24] R. Guzinski, H. Nieto, I. Sandholt, and G. Karamitilios, "Modelling high-resolution actual evapotranspiration through Sentinel-2 and Sentinel-3 data fusion," *Remote Sens.*, vol. 12, no. 9, 2020, Art. no. 1433.

[25] M. F. McCabe, D. G. Miralles, T. R. Holmes, and J. B. Fisher, "Advances in the remote sensing of terrestrial evaporation," *Remote Sens.*, vol. 11, no. 9, 2019, Art. no. 1138.

[26] H. Ma et al., "Satellite canopy water content from Sentinel-2, Landsat-8 and MODIS: Principle, algorithm and assessment," *Remote Sens. Environ.*, vol. 326, 2025, Art. no. 114801.

[27] F. Bernard et al., "The LSTM instrument: Design, technology and performance," *Proc. SPIE*, vol. 12777, pp. 1712–1729, 2023.

[28] J.-P. Lagouarde et al., "The Indian Trishna Mission: Earth observation in the thermal infrared with high spatio-temporal resolution," in *Proc. IEEE Int. Geosci. Remote Sens. Symp.*, IEEE, 2018, pp. 4078–4081.

[29] M. F. McCabe, B. Aragon, R. Houborg, and J. Mascaro, "CubeSats in hydrology: Ultrahigh-resolution insights into vegetation dynamics and terrestrial evaporation," *Water Resour. Res.*, vol. 53, no. 12, pp. 10017–10024, 2017.

[30] A. G. Konings, K. Rao, and S. C. Steele-Dunne, "Macro to micro: Microwave remote sensing of plant water content for physiology and ecology," *New Phytologist*, vol. 223, no. 3, pp. 1166–1172, 2019.

[31] P. C. Vermunt et al., "Response of subdaily L-band backscatter to internal and surface canopy water dynamics," *IEEE Trans. Geosci. Remote Sens.*, vol. 59, no. 9, pp. 7322–7337, Jan. 2020.

[32] S. Khabbazan, S. C. Steele-Dunne, P. C. Vermunt, L. Guerriero, and J. Judge, "The influence of surface canopy water on L-band backscatter from corn: A study combining detailed in situ data and the Tor Vergata radiative transfer model," *Sci. Remote Sens.*, vol. 9, 2024, Art. no. 100137.

[33] A. J. Purdy et al., "SMAP soil moisture improves global evapotranspiration," *Remote Sens. Environ.*, vol. 219, pp. 1–14, 2018.

[34] A. Loew, J. Peng, and M. Borsche, "High-resolution land surface fluxes from satellite and reanalysis data (HOLAPS v1.0): Evaluation and uncertainty assessment," *Geoscientific Model Develop.*, vol. 9, no. 7, pp. 2499–2532, 2016.

[35] D. G. Miralles, T. Holmes, R. De Jeu, J. Gash, A. Meesters, and A. Dolman, "Global land-surface evaporation estimated from satellite-based observations," *Hydrol. Earth System Sci.*, vol. 15, no. 2, pp. 453–469, 2011.

[36] D. Rains, H. Lievens, G. J. De Lannoy, M. F. McCabe, R. A. de Jeu, and D. G. Miralles, "Sentinel-1 backscatter assimilation using support vector regression or the water cloud model at European soil moisture sites," *IEEE Geosci. Remote Sens. Lett.*, vol. 19, 2021, Art. no. 4013105.

[37] B. Martens, R. A. De Jeu, N. E. C. Verhoest, H. Schuurmans, J. Kleijer, and D. G. Miralles, "Towards estimating land evaporation at field scales using GLEAM," *Remote Sens.*, vol. 10, no. 11, 2018, Art. no. 1720.

[38] Q. Zhang, S. Manzoni, G. Katul, A. Porporato, and D. Yang, "The hysteretic evapotranspiration—vapor pressure deficit relation," *J. Geophysical Research: Biogeosciences*, vol. 119, no. 2, pp. 125–140, 2014.

[39] H. Zheng, Q. Wang, X. Zhu, Y. Li, and G. Yu, "Hysteresis responses of evapotranspiration to meteorological factors at a diel timescale: Patterns and causes," *PLoS One*, vol. 9, no. 6, 2014, Art. no. e98857.

[40] J. A. Nelson, N. Carvalhais, M. Migliavacca, M. Reichstein, and M. Jung, "Water-stress-induced breakdown of carbon–water relations: Indicators from diurnal FLUXNET patterns," *Biogeosciences*, vol. 15, no. 8, pp. 2433–2447, 2018.

[41] J. Friesen, J. Lundquist, and J. T. Van Stan, "Evolution of forest precipitation water storage measurement methods," *Hydrological Processes*, vol. 29, no. 11, pp. 2504–2520, 2015.

[42] S. C. Steele-Dunne, J. Friesen, and N. Van De Giesen, "Using diurnal variation in backscatter to detect vegetation water stress," *IEEE Trans. Geosci. Remote Sens.*, vol. 50, no. 7, pp. 2618–2629, Jan. 2012.

[43] S. C. Steele-Dunne, H. McNairn, A. Monsivais-Huertero, J. Judge, P.-W. Liu, and K. Papathanassiou, "Radar remote sensing of agricultural canopies: A review," *IEEE J. Sel. Topics Appl. Earth Observ. Remote Sens.*, vol. 10, no. 5, pp. 2249–2273, Mar. 2017.

[44] A. G. Konings, Y. Yu, L. Xu, Y. Yang, D. S. Schimel, and S. S. Saatchi, "Active microwave observations of diurnal and seasonal variations of canopy water content across the humid African tropical forests," *Geophysical Res. Lett.*, vol. 44, no. 5, pp. 2290–2299, 2017.

[45] T. van Emmerik et al., "Water stress detection in the amazon using radar," *Geophysical Res. Lett.*, vol. 44, no. 13, pp. 6841–6849, 2017.

[46] P. C. Vermunt, S. C. Steele-Dunne, S. Khabbazan, J. Judge, and N. C. van de Giesen, "Extrapolating continuous vegetation water content to understand sub-daily backscatter variations," *Hydrol. Earth System Sci.*, vol. 26, no. 5, pp. 1223–1241, 2022.

[47] S. C. Steele-Dunne et al., "SLAINTE: A SAR mission concept for sub-daily microwave remote sensing of vegetation," in *Proc. 15th Eur. Conf. Synthetic Aperture Radar*. IEEE, 2024, pp. 870–872.

[48] J. Matar, M. Sanjuan-Ferrer, M. Rodriguez Cassola, S. C. Steele-Dunne, and F. De Zan, "A concept for an interferometric SAR mission with sub-daily revisit," in *Proc. 15th Eur. Conf. Synthetic Aperture Radar*. IEEE, 2024, pp. 18–22.

[49] R. Atlas, "Atmospheric observations and experiments to assess their usefulness in data assimilation," *J. Meteorological Soc. Japan. Ser. II*, vol. 75, no. 1B, pp. 111–130, 1997.

[50] R. N. Hoffman and R. Atlas, "Future observing system simulation experiments," *Bull. Amer. Meteorological Soc.*, vol. 97, no. 9, pp. 1601–1616, 2016.
[51] N. Holtzman, Y. Wang, J. D. Wood, C. Frankenberg, and A. G. Konings, "Constraining plant hydraulics with microwave radiometry in a land surface model: Impacts of temporal resolution," *Water Resour. Res.*, vol. 59, no. 11, 2023, Art. no. e2023WR035481.
[52] P. Hulsman, J. Keune, A. Koppa, J. Schellekens, and D. G. Miralles, "Incorporating plant access to groundwater in existing global, satellite-based evaporation estimates," *Water Resour. Res.*, vol. 59, no. 8, 2023, Art. no. e2022WR033731.
[53] A. J. Rutter, K. A. Kershaw, P. C. Robins, and A. J. Morton, "A predictive model of rainfall interception in forests, I. derivation of the model from observations in a plantation of Corsican pine," *Agricultural Meteorol.*, vol. 9, pp. 367–384, 1971.
[54] A. J. Rutter, A. J. Morton, and P. C. Robins, "A predictive model of rainfall interception in forests. II. generalization of the model and comparison with observations in some coniferous and hardwood stands," *J. Appl. Ecol.*, vol. 12, pp. 367–380, 1975.
[55] B. Martens et al., "GLEAM v3: Satellite-based land evaporation and root-zone soil moisture," *Geoscientific Model Develop.*, vol. 10, no. 5, pp. 1903–1925, 2017.
[56] C. H. B. Priestley and R. J. Taylor, "On the assessment of surface heat flux and evaporation using large-scale parameters," *Monthly Weather Rev.*, vol. 100, no. 2, pp. 81–92, 1972.
[57] H. Lievens, B. Martens, N. E. C. Verhoest, S. Hahn, R. H. Reichle, and D. G. Miralles, "Assimilation of global radar backscatter and radiometer brightness temperature observations to improve soil moisture and land evaporation estimates," *Remote Sens. Environ.*, vol. 189, pp. 194–210, 2017.
[58] F. Zhong, S. Jiang, A. I. van Dijk, L. Ren, J. Schellekens, and D. G. Miralles, "Revisiting large-scale interception patterns constrained by a synthesis of global experimental data," *Hydrol. Earth System Sci.*, vol. 26, no. 21, pp. 5647–5667, 2022.
[59] R. Tamrakar, M. B. Rayment, F. Moyano, M. Mund, and A. Knohl, "Implications of structural diversity for seasonal and annual carbon dioxide fluxes in two temperate deciduous forests," *Agricultural Forest Meteorol.*, vol. 263, pp. 465–476, 2018.
[60] Warm Winter 2020 Team, & ICOS Ecosystem Thematic Centre, "Warm winter 2020 ecosystem eddy covariance flux product for 73 stations in FLUXNET-Archive format—release 2022-1," ICOS Carbon Portal, 2022, doi: 10.18160/2G60-ZHAK.
[61] G. Pastorello et al., "The FLUXNET2015 dataset and the ONEFlux processing pipeline for eddy covariance data," *Sci. Data*, vol. 7, no. 1, pp. 1–27, 2020.
[62] S. Rambal et al., "Drought controls over conductance and assimilation of a Mediterranean evergreen ecosystem: Scaling from leaf to canopy," *Glob. Change Biol.*, vol. 9, no. 12, pp. 1813–1824, 2003.
[63] H. Hersbach et al., "The ERA5 global reanalysis," *Quart. J. Roy. Meteorological Soc.*, vol. 146, no. 730, pp. 1999–2049, 2020.
[64] K. Luojus, J. Pulliainen, M. Takala, J. Lemmetyinen, and M. Moisander, "GlobSnow v3.0 snow water equivalent (SWE)," 2020, doi: 10.1594/PANGAEA.911944.
[65] L. Moesinger et al., "The global long-term microwave Vegetation Optical Depth Climate Archive (VODCA)," *Earth Syst. Sci. Data*, vol. 12, no. 1, pp. 177–196, 2020.
[66] G. Simons, R. Koster, and P. Droogers, "HiHydroSoil v2.0 - high resolution soil maps of global hydraulic properties," 2020, FutureWater Rep. 213. [Online]. Available: https://www.futurewater.eu/projects/hihydrosoil
[67] Global Soil Data Task Group, "Global gridded surfaces of selected soil characteristics (IGBP-DIS)," distributed by NASA Oak Ridge National Laboratory DAAC, 2000, doi: 10.3334/ORNLDAAC/569.
[68] C. DiMiceli, M. Carroll, R. Sohlberg, D. Kim, M. Kelly, and J. Townshend, MOD44B MODIS/Terra vegetation continuous fields yearly L3 global 250 m SIN grid V006, distributed by NASA EOSDIS Land Processes DAAC, 2015, doi: 10.5067/MODIS/MOD44B.006.
[69] M. Hansen and X. Song, "VCF5KYR MEaSUREs vegetation continuous fields (VCF) yearly global 0.05 deg V001," distributed by NASA EOSDIS Land Processes DAAC, 2018, doi: 10.5067/MEaSUREs/VCF/VCF5KYR.001.
[70] R. Myneni, Y. Knyazikhin, and T. Park, "MCD15A3H MODIS/Terra aqua leaf area Index/FPAR 4-day L4 global 500 m SIN grid V006," distributed by NASA EOSDIS Land Processes DAAC, 2015, doi: 10.5067/MODIS/MCD15A3H.006.
[71] N. M. Holtzman et al., "L-band vegetation optical depth as an indicator of plant water potential in a temperate deciduous forest stand," *Biogeosciences*, vol. 18, no. 2, pp. 739–753, 2021.
[72] M. Momen et al., "Interacting effects of leaf water potential and biomass on vegetation optical depth," *J. Geophysical Res.: Biogeosciences*, vol. 122, no. 11, pp. 3031–3046, 2017.
[73] Global climate observing system (GCOS), "The 2022 GCOS ECVs requirements," 2022. [Online]. Available: https://library.wmo.int/idurl/4/58111
[74] B. Martens, D. G. Miralles, H. Lievens, D. Fernández-Prieto, and N. E. C. Verhoest, "Improving terrestrial evaporation estimates over continental Australia through assimilation of SMOS soil moisture," *Int. J. Appl. Earth Observation Geoinformation*, vol. 48, pp. 146–162, 2016.
[75] B. Chen, T. A. Black, N. C. Coops, T. Hilker, J. Trofymow, and K. Morgenstern, "Assessing tower flux footprint climatology and scaling between remotely sensed and eddy covariance measurements," *Boundary-Layer Meteorol.*, vol. 130, no. 2, pp. 137–167, 2009.
[76] M. Göckede et al., "Quality control of CarboEurope flux data–Part 1: Coupling footprint analyses with flux data quality assessment to evaluate sites in forest ecosystems," *Biogeosciences*, vol. 5, no. 2, pp. 433–450, 2008.
[77] M. Mauder, M. Jung, P. Stoy, J. Nelson, and L. Wanner, "Energy balance closure at FLUXNET sites revisited," *Agricultural Forest Meteorol.*, vol. 358, 2024, Art. no. 110235.
[78] W. Zhang et al., "A new post-hoc method to reduce the energy imbalance in eddy covariance measurements," *Geophysical Res. Lett.*, vol. 51, no. 2, 2024, Art. no. e2023GL107084.
[79] W. H. Maes, P. Gentine, N. E. C. Verhoest, and D. G. Miralles, "Potential evaporation at eddy-covariance sites across the globe," *Hydrol. Earth System Sci.*, vol. 23, no. 2, pp. 925–948, 2019.
[80] R. M. Bright, D. G. Miralles, R. Poyatos, and S. Eisner, "Simple models outperform more complex big-leaf models of daily transpiration in forested biomes," *Geophysical Res. Lett.*, vol. 49, no. 18, 2022, Art. no. e2022GL100100.
[81] V. Humphrey and C. Frankenberg, "Continuous ground monitoring of vegetation optical depth and water content with GPS signals," *Biogeosciences*, vol. 20, pp. 1789–1811, 2023.
[82] D. G. Miralles et al., "GLEAM4: Global land evaporation and soil moisture dataset at 0.1 resolution from 1980 to near present," *Sci. Data*, vol. 12, no. 1, 2025, Art. no. 416.
[83] A. T. Schackow, S. C. Steele-Dunne, D. T. Milodowski, J.-M. Limousin, and A. Bastos, "Vegetation health monitoring based on sub-daily sap flow variability," *EGUsphere*, vol. 2025, pp. 1–34, 2025.

Emma Tronquo received the M.Sc. and Ph.D. degrees in bioscience engineering from Ghent University, Ghent, Belgium, in 2019 and 2024, respectively.

She is currently a postdoctoral Researcher with the Department of Geoscience and Remote Sensing, Delft University of Technology, Delft, The Netherlands; and with the Hydro-Climate Extremes Lab (H-CEL), Ghent University. Her research interests lie in microwave–vegetation interactions and sub-daily remote sensing, with a focus on radar-based estimation of soil moisture and evaporation.

Hans Lievens received the M.Sc. and Ph.D. degrees in bioscience engineering from Ghent University, Ghent, Belgium, in 2007 and 2011, respectively.

From 2012 to 2018, he was a Postdoctoral Research Fellow with the Flemish Research Foundation (FWO). During this fellowship, he spent one year (2016–2017) as a Visiting Research Scientist with the Global Modeling and Assimilation Office (GMAO) of NASA Goddard Space Flight Center, Greenbelt, MD, USA. Between 2018 and 2022, he was a Postdoctoral Researcher with KU Leuven, Belgium, and since 2022, he has been a Post-doctoral Assistant with H-CEL, Ghent University, contributing to teaching activities on hydrological modeling and advanced remote sensing, and supervising research projects related to remote sensing, modeling, and data assimilation applied to snow.

Susan C. Steele-Dunne received the S.M. and Ph.D. degrees in hydrology from the Massachusetts Institute of Technology, Cambridge, MA, USA, in 2002 and 2006, respectively.

She has been with the Faculty of Civil Engineering and Geosciences, Delft University of Technology, Delft, The Netherlands, since 2008. She leads the M-WAVE group, who perform research from field to global scales, combining in situ and spaceborne sensors to improve our understanding of microwave interactions with vegetation. Her research interests include the use of data assimilation, modeling, and machine learning to exploit spaceborne radar instruments for applications in ecosystem and agricultural monitoring.

Niko E. C. Verhoest received the engineering and the Ph.D. degrees in applied biological sciences, from Ghent University, Ghent, Belgium, in 1994 and 2000, respectively.

He was a Teaching Assistant and an Assistant Professor with the Laboratory of Hydrology and Water Management (currently H-CEL), Ghent University, from 1998 to 2000 and 2000 to 2002, respectively. In 2002, he became Associate Professor of Hydrology and Water Management with the Faculty of Bioscience Engineering, Ghent University. He is (co-)responsible for several courses taught at the Faculty of Bioscience Engineering. His research interests focus on three main pillars: application of remotely sensed observations in hydrological models (including retrieval algorithms, hydrological modeling, and data assimilation), stochastic hydrology, and ecohydrology.

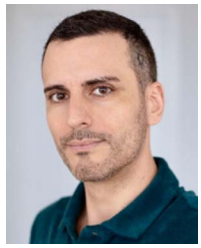

Diego G. Miralles received the M.Sc. and Ph.D. degrees in hydrology from VU Amsterdam, Amsterdam, The Netherlands, in 2009 and 2011, respectively.

He became Professor in Hydrology and Climate with Ghent University, Ghent, Belgium, in 2017, after a journey via the U.K., the Netherlands, and the USA. He leads the Hydrology and Climate team at H-CEL which is dedicated to the understanding how the hydrosphere, biosphere and climate interact and the implications for current and future societies.

Prof. Miralles is the recipient of ERC Starting and Consolidator grants and a Clarivate Highly Cited Researcher. He specializes in ecohydrology, land–atmosphere interactions, global hydrology, hydro-climatic extremes, and satellite remote sensing.